

Modeling Neural Networks with Privacy Using Neural Stochastic Differential Equations

Sanghyun Hong*, Fan Wu†, Anthony Gruber‡, Kookjin Lee†,

*Oregon State University

†Arizona State University

‡Sandia National Laboratories

Abstract—In this work, we study the feasibility of using neural ordinary differential equations (NODEs) to model systems with intrinsic privacy properties. Unlike conventional feedforward neural networks, which have unlimited expressivity and can represent arbitrary mappings between inputs and outputs, NODEs constrain their learning to the solution of a system of differential equations. We first examine whether this constraint reduces memorization and, consequently, the membership inference risks associated with NODEs. We conduct a comprehensive evaluation of NODEs under membership inference attacks and show that they exhibit twice the resistance compared to conventional models such as ResNets. By analyzing the variance in membership risks across different NODE models, we find that their limited expressivity leads to reduced overfitting to the training data. We then demonstrate, both theoretically and empirically, that membership inference risks can be further mitigated by utilizing a stochastic variant of NODEs: neural stochastic differential equations (NSDEs). We show that NSDEs are differentially-private (DP) learners that provide the same provable privacy guarantees as DP-SGD, the de-facto mechanism for training private models. NSDEs are also effective in mitigating membership inference attacks, achieving risk levels comparable to private models trained with DP-SGD while offering an improved privacy-utility trade-off. Moreover, we propose a drop-in-replacement strategy that efficiently integrates NSDEs into conventional feedforward architectures to enhance their privacy.

1. Introduction

Neural networks are “universal function approximators”: they can learn arbitrary continuous mappings from training data to target outputs [1]. This expressivity allows highly parameterized networks to model complex, non-linear relationships and capture hidden patterns that traditional methods may struggle to detect. However, this strength also introduces an undesirable property: *memorization* [2]. Memorization occurs when the learned mappings are overly specific to individual training instances—regardless of whether these mappings generalize to unseen data—potentially leading to the leakage of their membership through model queries [3], [4], [5], [6], [7]. Given that neural networks are often deployed in sensitive domains, such as healthcare, where

training data may include confidential medical records, this membership leakage naturally raises privacy concerns.

Recent work has introduced a new class of neural networks: neural ordinary differential equations (NODEs) [8]. Unlike conventional neural networks, NODEs constrain the learned mappings to solutions of parameterized differential equations—a fundamental mathematical tool for describing processes in the physical world. By shifting from manually designing governing equations to data-driven modeling, NODEs have emerged as a powerful paradigm in scientific computing for modeling dynamical systems across various domains, such as time-series forecasting [9], [10], [11], scientific machine learning (ML) [12], [13], [14], [15], and computer vision tasks [16], [17], [18], [19]. These works demonstrate that NODEs, despite their constrained expressivity to learnable differential equations, can achieve performance comparable to that of conventional neural networks across a range of tasks.

In this work, we study the privacy implications of employing differential equation-based neural networks. Specifically, we ask the following research question: *Does this emerging class of neural networks (and their variants) offer inherent privacy advantages, such as reduced membership inference risks, compared to conventional neural networks?* Because NODEs restrict model expressivity to the system of differential equations, they may influence memorization and overfitting—key factors attributing to membership inference risks. Their stochastic variants, neural stochastic differential equations (NSDEs), introduce randomness into the model dynamics and thus, may satisfy formal privacy guarantees. Moreover, the modular design of these models could enable their integration into conventional feedforward architectures as privacy-enhancing components.

We first conduct a systematic evaluation of the membership inference risks associated with NODEs. To this end, we develop a risk analysis framework that runs six off-the-shelf membership inference attacks across a variety of neural networks including NODEs and baseline feedforward models. In our evaluation on four image recognition benchmarks, commonly used in prior work on assessing membership risks, we find that NODEs exhibit up to $2\times$ lower membership risks compared to conventional feedforward networks, like ResNets [20]. We also find that this reduced risk is partly attributable to the lower degree of overfitting in

NODEs, while achieving accuracy comparable to baselines.

Moreover, we analyze factors that may affect their membership risks. We first examine configurations one can control at the block-level: solvers, tolerance, and step size. Our analysis indicates that these factors, which change the complexity of learned dynamics while keeping the same model capacity, can increase/decrease the likelihood of overfitting. We also test the model-level configurations: the number of blocks and advanced variants of NODEs [16], [18], [21]. They increase the model capacity or the complexity of learned dynamics, and therefore, increase membership risks.

Our previous evaluation shows that, while NODEs are less vulnerable, the risks to membership inference still exist. We address this problem by employing a stochastic adaptation of NODEs: NSDEs [22]. NSDEs also model underlying dynamics using differential equations, but augment them with a diffusion term that introduces Gaussian noise.

We first formally show that this diffusion term acts as a differentially-private (DP) mechanism during training, and turns NSDEs into DP-learners. We establish a theoretical bound on privacy leakage per mini-batch SGD iteration and present a mechanism to account for total privacy leakage over the entire training process. Surprisingly, we find that the total privacy leakage (ϵ) guaranteed by NSDE training matches that of DP-SGD [23], the de-facto standard for training private models. The leakage ϵ is proportional to the number of training iterations and the noise level (σ).

We then empirically evaluate the effectiveness of NSDEs in further reducing the membership inference risks. Our results show that NSDEs reduce the effectiveness of existing membership inference attacks by 1.8–10 \times compared to NODEs. Despite offering the same privacy guarantee, NSDE models maintain utility that is comparable to (or slightly higher than) ResNet models trained with DP-SGD. This shows NSDEs as a promising countermeasure that achieves an improved privacy-utility trade-off. We also compare NSDEs with prior heuristic defenses [24] designed to counter membership inference attacks but lacking formal privacy guarantees. We show that NSDEs are 2–5 \times more effective in mitigating the membership inference risks.

Implementing our privacy mechanism requires training an NSDE model from scratch, which can be a computationally demanding option for model providers. To address this practical challenge, we propose an effective strategy to apply NSDEs to existing pre-trained models, particularly conventional model architectures like ResNets. We leverage the common practice of *transfer learning* where the last layer of a pre-trained model is replaced with a classification head, followed by fine-tuning on data for a few iterations. Our proposed strategy, *replace-then-finetune*, substitutes the last few layers of a pre-trained model with an NSDE block. We test our strategy on ResNet14 pre-trained on the four benchmark tasks. Across all benchmarks, the fine-tuned models maintain accuracy comparable to the pre-trained models, while reducing the membership risks substantially (e.g., by 10 \times in CIFAR-10). We hope our work encourages the adoption of NSDEs as a viable mechanism for further reducing privacy risks while maintaining model utility.

Contributions. In summary, our contributions are:

- We are the first to study the membership inference risks of NODEs. Our comprehensive evaluation shows that NODEs exhibit 2 \times lower membership risks compared to baseline models. We attribute this to NODEs’ reduced overfitting, which is from their restricted expressivity—learning within the constraints of a system of ODEs.
- We propose NSDEs as a defense mechanism to mitigate membership inference attacks. We formally show that NSDEs provide the same provable privacy guarantee as DP-SGD. We also present an accounting mechanism to track the total privacy leakage during NSDE training.
- In our evaluation, we show that NSDEs reduce membership inference risks by 2–5 \times compared to heuristic defenses without provable guarantees. Compared to private models trained with DP-SGD, NSDEs offer comparable (provable) protection against membership inference attacks while achieving slightly higher accuracy.
- We present a practical strategy to leverage these privacy benefits without fully replacing existing models with NSDEs: *replace-then-finetune*. This strategy reduces membership inference risks by 10 \times while achieving a higher utility than private models trained with DP-SGD.

2. Background

2.1. Neural Ordinary Differential Equations

NODEs model the dynamics of system states as a system of ODEs such that:

$$\frac{d\mathbf{h}(t)}{dt} = \mathbf{f}_\Theta(\mathbf{h}(t), t),$$

where $\mathbf{h}(t)$ are the state variables and \mathbf{f}_Θ is a neural network, parameterized by its parameters Θ , defining the rate of change in $\mathbf{h}(t)$. The scalar variable t refers to a time variable and the system states correspond to observables in time-dependent physical processes [25] or measurements in time-series data (e.g., [26]). However, in the context of hidden representations within a deep feedforward network (FFN), t instead refers to a continuous depth parameter. More precisely, recall that the flow map $\varphi = \varphi(t, \mathbf{h})$ of an ODE system associates to each state \mathbf{h} its “flowed out” state after evolving along the ODE for t time, i.e., $\varphi(0, \mathbf{h}) = \mathbf{h}$ and $(d/dt)\varphi(t, \mathbf{h}) = \mathbf{f}_\Theta(\mathbf{h}(t), t)$ in the case of the NODE above. Then, the number of “layers” in the NODE architecture defined by \mathbf{f}_Θ is analogous to the number of “time steps” used to generate the flowed-out state $\mathbf{h}(t)$, and hence each network prediction based on this quantity. Our focus is on this use case, which allows for depth control through direct manipulation of the ODE time-stepping.

Training and inference. In NODEs, the forward pass involves solving an initial value problem (IVP) describing the evolution of some given initial states under the flow of the learnable ODE in question. Given an initial condition $\mathbf{h}(0) = \mathbf{h}_0$ for the state variables (or hidden state representations), the states at any time index $\{\mathbf{h}(t_i)\}_{i=1}^n$ can

be obtained by solving the associated IVP, lending NODEs their interpretation as continuous-depth FFNs. To solve the necessary IVP, a black-box ODE time-integrator with solver options OPT can be employed:

$$\mathbf{h}(t_1), \dots, \mathbf{h}(t_n) = \text{ODESolve}(\mathbf{f}_\Theta, \mathbf{h}(0), [t_1, \dots, t_n], \text{OPT}).$$

Different choices of numerical time-integration yield different realizations of FFNs, e.g., under the forward Euler method with step size 1, autonomous (t -independent) NODEs degenerate to ResNets [20], $\mathbf{h}(t_{i+1}) = \mathbf{h}(t_i) + \mathbf{f}_\Theta(\mathbf{h}(t_i))$. With this setup, the forward pass for both training and inference is equivalent to recurrently applying a nonlinear transformation, defined by \mathbf{f}_Θ , to a hidden state, followed by a skip connection. In classification tasks, the last hidden representation $\mathbf{h}(t_n)$ is fed into a classifier network, producing logits, and the loss of the model is obtained via computing the cross-entropy. The continuous-depth network $\mathbf{M}(t, \mathbf{h}) = \mathbf{M}_t(\mathbf{h}) \approx \varphi(t, \mathbf{h})$ can then be thought of as discretizing the ODE flow map, i.e., $\mathbf{M}_{t_n}(\mathbf{h}_0) = \mathbf{h}(t_n)$, where $\mathbf{h}(t_n)$ is the solution of the IVP defined above. As mentioned before, any intermediate time steps t_1, \dots, t_{n-1} used in the production of the final state $\mathbf{h}(t_n)$ are analogous to the labels on hidden layers in an FFN.

For the backward process required during training, NODEs use either standard backpropagation through the rolled-out computational path, or the adjoint sensitivity method [27]. The primary challenge lies in achieving stable and memory-efficient gradient computation for \mathbf{f}_Θ with respect to its parameters, as backpropagating directly through an iterative numerical solver can be memory intensive and exacerbate vanishing or exploding gradient issues.

NODE variants. Many variants have been developed to improve their expressivity and efficiency. Augmented NODEs (ANODEs) [16] propose an additional dimension to the state variable $[\mathbf{h}(t), \mathbf{a}(t)]$, to increase expressivity. ANODEs were further extended into second-order NODEs (SONODEs) [21], which formulates a system of coupled first-order NODEs, implementing the broader class of augmented models. Other variants incorporate concepts from gradient descent optimization, such as momentum, resulting in heavy ball NODEs (HBNODEs) [18] and Nesterov NODEs [28], both of which improve computational efficiency by reducing the number of function evaluations in the forward pass.

NSDEs [22], [29], [30] extend NODEs to the modeling of stochastic processes, typically introducing randomness in the form of additive Gaussian noise. These systems can be formulated in terms of deterministic, vector-valued “drift” and stochastic, matrix-valued “diffusion” terms as follows:

$$d\mathbf{h} = \mathbf{f}_{\Theta_1}(\mathbf{h}, t) dt + \mathbf{G}_{\Theta_2}(\mathbf{h}, t) d\mathbf{B}_t,$$

where $d\mathbf{B}_t$ denotes the Wiener increment—a zero mean, unit variance, delta-correlated Gaussian process describing “white noise”. A simple but popular discretization of NSDEs is given by the Euler–Maruyama method [31] with step size 1, expressed as $\mathbf{h}(t_{i+1}) = \mathbf{h}(t_i) + \mathbf{f}_{\Theta_1}(\mathbf{h}, t_i)\Delta t + \mathbf{G}_{\Theta_2}(\mathbf{h}, t_i)\mathbf{w}_{t_i}$, where Δt is the time step size and $\mathbf{w}_{t_i} \sim$

$\mathcal{N}(0, \Delta t)$ is randomly sampled. In this formulation, Gaussian noise is injected alongside each residual connection. Because of this property, NSDEs have shown enhanced robustness against adversarial examples [32] compared to standard NODEs. Our study further explores this property as a formal mechanism for mitigating privacy risks.

2.2. Membership Inference Attacks

Membership inference attacks aim to determine whether a specific sample is a *member* of the training data. To do this, the attacker exploits the difference in the target model’s response to the specific sample when it is a member versus a non-member. Membership inference can be considered a threat on its own, but a model’s vulnerability to inference attacks also implies its potential to leak other private information outside of this context, an idea which aligns closely with the definition of differential privacy [33].

Existing attacks. Prior work has developed various attacks to exploit differences and identify *membership*. In our work, we evaluate NODEs against each of the representative attacks described below:

- Yeom *et al.* [3] focus on differences in *loss* values: for a specific instance $z = (x, y)$, a model will be more accurate in its predictions when it has seen z during training. The attack predicts z as a member if and only if, for a threshold τ , the model’s loss on z is below τ ; otherwise, it is classified as a non-member.
- Shokri *et al.* [4] leverage *shadow models* which better approximate the differences in a model’s responses to members versus non-members. When constructing shadow models, the attacker artificially generates datasets for training and testing so that the members and non-members are known in advance. The attacker collects responses from shadow models for both members and non-members and trains a classifier to predict membership of z based on the target model’s response.
- Song and Mittal [5] leverage the *prediction correctness* to compute the threshold τ for identifying membership. Instead of training classifiers to perform attacks, τ is designed such that correct predictions with high confidence yield the lowest values while confident but incorrect predictions achieve the highest.
- Watson *et al.* [34] proposed *per-example difficulty* calibration in which an attacker leverages shadow models trained without a particular example to compute the average confidence level of a model. The average is then subtracted from the example’s confidence obtained from the target model to calibrate the difficulty of the sample.
- Carlini *et al.* [6] introduced Likelihood Ratio Attack (LiRA), which refines how shadow training data is used by the adversary. For each sample in the shadow training data, LiRA trains two sets of shadow models: one set with the sample included (“in”) and another without (“out”). The attacker collects logits from both members and non-members across these shadow models, computes a membership score for a sample z as the ratio of the

likelihoods of observing its logit in “in” versus “out” models, and uses this score to identify membership.

- The latest work by Zarifzade *et al.* [35] introduced a Robust Membership Inference Attack (RMIA), which models membership inference as a fine-grained likelihood-ratio test. RMIA operates by contrasting the target model’s output distribution against a reference distribution, constructed from a small set of reference models and population data. This approach enables more robust differentiation between members and non-members.

Metrics. Initial work [3] uses inference accuracy as a metric for evaluating attack success. Subsequent works use the area under the ROC curve (AUC) as an additional metric to report the balance between true-positive (TPR) and false-positive rates (FPR). More recently, Carlini [6] proposes evaluating attack success in the worst-case *low-FPR regime*. Our work reports all these metrics in evaluation.

2.3. Defenses against Membership Inference

Prior work has developed defenses to obscure the difference in model output between members and non-members.

Reducing overfitting. One key difference is the degree of overfitting or the extent to which a model memorizes its training data. Yeom *et al.* [3] found that defending against membership inference attacks and reducing overfitting go hand-in-hand, so that the goals of privacy and performance are aligned. Many defenses [4], [5], [36] therefore focus on a regularization effect, and existing regularization methods are also being used to reduce membership risk [24].

- ℓ^p -regularization and dropout are two of the most commonly used regularization techniques in practice, shown effective against membership inference attacks [4].
- *Early stopping* is a straightforward way to prevent overfitting [5]. One halts training when the model’s performance stops improving. This has the effect of stopping the model before it can begin to memorize.
- *MMD with Mix-up* [37] combines two different mechanisms: (1) a maximum mean discrepancy (MMD) loss to reduce the training accuracy to match validation accuracy, and (2) training on mix-up augmented data, where a linear interpolation between two randomly drawn examples (and their labels) is used instead of individual samples. Mix-up has been shown to increase overall accuracy and further reduce overfitting.
- *MemGuard* [36] uses an “attack-as-a-defense” approach: It adds carefully-calibrated noise to each confidence score vector predicted by the target model. Once added, the resulting adversarial examples mislead the attacker’s membership identification (e.g., the attack classifiers).

Differential privacy [33] (DP) is a mathematical framework that provides a probabilistic privacy guarantee. Precisely, the following definition implies that, as a random variable, the privacy loss is bounded in the worst case by a constant $\epsilon > 0$ with probability $0 < 1 - \delta < 1$.

Definition 2.1 ((ϵ, δ) -DP). Given any two datasets D and D' that differ by only a single record, a mechanism M satisfies (ϵ, δ) -DP if, for any subset S of the image of M ,

$$Pr[M(D) \in S] \leq e^\epsilon Pr[M(D') \in S] + \delta$$

where ϵ is the privacy budget (or leakage) and δ is the failure probability.

A primary advantage of DP is its immunity to post-processing: an (ϵ, δ) -DP algorithm cannot be weakened through manipulation of its output. Based on this property, Abadi *et al.* proposed an effective, differentially-private adaptation of stochastic gradient descent: DP-SGD [23]. The key in DP-SGD is the *moment accountant*, a mechanism that tracks total privacy leakage possible under a worst-case adversary. This leakage is typically denoted as ϵ , a convention that will be followed throughout the rest of the paper. Because of the formal privacy guarantee that DP-SGD offers, it has become a de-facto standard for constructing private models. However, this approach inherently leads to a utility loss due to the addition of Gaussian noise to the gradients required for accurate learning. We evaluate how effective those defenses are in mitigating the membership risks of NODEs and formally demonstrate that NSDEs are DP learners, offering an improved privacy-utility tradeoff.

3. Membership Risks of NODEs

We first evaluate the membership risks of NODEs. Our hypothesis is that these models are vulnerable to existing membership inference attacks as their performance on popular benchmarking tasks is comparable to conventional feedforward networks. However, because their expressivity is limited to modeling a system of ODEs, the risk could be lower than that of conventional networks.

3.1. Threat Model

The attacker aims to determine whether a specific sample $z = (x, y)$ is included in the data used for training the target model f . The adversary only has *black-box* access to f .¹ We assume that the attacker can train shadow models f_s with known membership for all shadow training samples and use them to infer membership from the model output. Because the attacker aims for f_s to closely resemble the behaviors of f , we assume the attacker’s shadow training dataset and the original training data come from the same underlying data distribution and may overlap partially. We also assume a worst-case black-box adversary with full knowledge of f ’s architecture and training configurations such that they employ this knowledge to construct and train f_s . When evaluating defenses in §5, we consider an *adaptive* adversary who knows the defense mechanisms deployed on f and their hyper-parameters.

1. Nasr *et al.* [39] showed that a *white-box* membership adversary with full access to the model and its parameters, does not particularly perform better than black-box attacks.

TABLE 1. COMPARISON OF MEMBERSHIP INFERENCE RISKS. WE EVALUATE TWO DIFFERENT TYPES OF NEURAL NETWORKS AGAINST SIX EXISTING ATTACKS ON FOUR BENCHMARKS. WE COMPARE THEIR RISKS BASED ON FOUR DIFFERENT METRICS USED IN THE PRIOR WORK.

Model	Method	TPR @ 0.1% FPR				TPR @ 1% FPR				AUC				Inference acc.			
		F-M	C-10	C-100	T-I	F-M	C-10	C-100	T-I	F-M	C-10	C-100	T-I	F-M	C-10	C-100	T-I
ResNet-14	Yeom et al. [3]	0.00%	0.00%	0.00%	0.02%	0.00%	0.00%	0.69%	1.11%	0.563	0.590	0.767	0.683	59.91%	58.92%	73.81%	64.27%
	Shokri et al. [4]	0.05%	0.01%	0.01%	0.10%	0.50%	0.14%	0.06%	1.01%	0.468	0.411	0.336	0.501	50.00%	50.00%	50.00%	50.42%
	Song and Mittal [38]	0.00%	0.00%	0.25%	0.13%	0.23%	0.00%	1.76%	1.23%	0.471	0.590	0.494	0.499	51.29%	58.92%	51.19%	50.28%
	Watson et al. [34]	0.00%	0.00%	0.00%	0.12%	0.00%	0.00%	0.62%	1.21%	0.554	0.590	0.767	0.548	56.21%	58.92%	73.81%	53.43%
	Carlini et al. [6]	1.92%	3.96%	10.52%	0.28%	5.87%	10.57%	25.95%	1.97%	0.599	0.679	0.865	0.554	55.70%	61.15%	76.46%	53.72%
	Zarifzadeh et al. [35]	1.13%	3.73%	13.98%	0.32%	6.54%	8.78%	28.25%	2.25%	0.497	0.581	0.858	0.578	56.83%	59.13%	75.53%	55.39%
NODE	Yeom et al. [3]	0.00%	0.00%	0.01%	0.09%	0.06%	0.00%	0.71%	1.12%	0.518	0.558	0.701	0.645	52.55%	56.59%	70.75%	61.23%
	Shokri et al. [4]	0.09%	0.04%	0.04%	0.10%	0.90%	0.43%	0.37%	1.01%	0.493	0.448	0.398	0.502	50.15%	50.01%	50.00%	50.21%
	Song and Mittal [38]	0.00%	0.00%	0.15%	0.12%	0.53%	0.00%	1.66%	1.19%	0.507	0.529	0.498	0.500	50.98%	54.22%	52.48%	50.45%
	Watson et al. [34]	0.00%	0.00%	0.01%	0.12%	0.04%	0.00%	0.71%	1.17%	0.517	0.558	0.701	0.542	52.04%	56.69%	70.75%	53.24%
	Carlini et al. [6]	0.19%	1.01%	3.30%	0.24%	1.48%	4.22%	12.11%	1.74%	0.529	0.616	0.782	0.543	52.81%	57.65%	72.88%	52.95%
	Zarifzadeh et al. [35]	0.67%	1.93%	5.41%	0.26%	3.16%	6.57%	17.58%	2.04%	0.523	0.592	0.797	0.570	53.05%	58.17%	73.37%	55.04%

3.2. Experimental Setup

Datasets. We use four object recognition benchmarks: FashionMNIST [40], CIFAR-10 and CIFAR-100 [41], and Tiny-ImageNet [42]. These datasets are commonly employed in prior work [3], [4], [6], [38]. We employ them to evaluate and compare the membership risks of NODEs with those reported in prior studies on feedforward neural networks.

Models. For each dataset, we train models with architectures based on those studied by Oganessian *et al.* [43]. They have a first few convolutional layer for downsampling, followed by three residual or ODE blocks (see Appendix for details). Our baseline is a ResNet architecture (**ResNet-14**) with 3 residual blocks where each block within a group has the same size and each group has 16, 32, and 64 filters respectively, widened by a factor of 2. To construct our NODE models, we substitute each group of residual blocks with an ODE block. **NODE** (ODENet-16-32-64) uses the same dimensions. We also examine **ODENet-64**, which contains only one ODE block after the downsampling layers—a typical structure used in prior work [8], [16].

Metrics. Following best practices from prior work [6], we measure the membership risks by computing the true-positive rate at a low false-positive rate ($TPR@0.1-1\%$ FPR). We also compare AUC and inference accuracy (or accuracy). Because this empirical membership risk is highly connected to a model’s generalization gap, we report both the best train and test accuracies of target models.

3.3. Quantifying the Membership Risks

We evaluate our models against six membership inference attacks outlined in §2.2. For the attacks employing shadow models, we train 16 models on 16 different subsets of the original training dataset. Following the strategy of prior work [6], we construct these 16 different shadow training datasets such that each training sample is included in half of the sets and excluded from the other half. We then choose one of them as the target model f and the remaining 15 as shadow models f_s . We run 16-fold cross-validation by choosing a different target model from the 16 models in each round, and we report the averaged metrics. For attacks like those by Yeom *et al.*, which do not use shadow models.

Results. Table 1 summarizes our results. Due to the page limit, we include the ODENet-64 results in Appendix and focus on ResNet-14 and NODE models. We contrast the membership risks of NODEs and ResNet-14 models. Overall, we find that *NODEs are 2× less vulnerable to membership inference attacks*, compared to ResNet14 in most cases. In CIFAR-10, attacks except those by Carlini *et al.* and Zarifzadeh *et al.* show a TPR of $\sim 0.0\%$ at 0.1–1.0% FPR. Against the two effective attacks, NODEs reduce their effectiveness by 1.3–4× than ResNet-14. On CIFAR-100, other attacks also show some effectiveness, with TPRs of up to 1.5%, but the LiRA and RMIA attacks remain the most effective. Both attacks are 1.6–2.6× less effective on NODEs at the same low-FPR regime. On FashionMNIST and Tiny-ImageNet, we also observe a reduction in membership inference success. However, as the baseline attacks were already less effective on these datasets, the relative reduction is limited at most 2×. We find the reduced effectiveness in AUC and inference accuracy. Note that our results do not imply that NODEs are free from membership risks. The attacks are still effective, with TPRs ranging from 1.1% to 10.6% at low FPRs in CIFAR-10 and 100.

Generalization gap is a known factor contributing to membership risks. Prior work [3], [4] shows that risks increase when a model *overfits*—it shows a large disparity between the training and testing accuracy. Hence, we analyze whether the reduced membership risks observed in NODEs are because of lower overfitting. Table 2 summarizes the gaps.

TABLE 2. GENERALIZATION GAP, MEASURED FOR BOTH RESNET-14 AND NODE MODELS ACROSS FOUR BENCHMARK DATASETS.

Task	F-M		C-10		C-100		T-I	
Model	R-14	NODE	R-14	NODE	R-14	NODE	R-14	NODE
Train	100.0%	95.5%	98.1%	94.3%	95.0%	82.1%	64.7%	55.9%
Test	88.4%	90.0%	86.0%	84.4%	54.3%	52.2%	42.4%	40.5%
Δ	11.6%	5.5%	12.1%	9.9%	40.7%	29.9%	22.3%	15.4%

Figure 1 analyzes the interaction between membership risks and the generalization gap in CIFAR-10. We plot the attack success and the generalization gap observed for each of the 16 target models, focusing on LiRA [6], where we observe the largest reduction. We first find that overfitting correlates with the success of membership inference attacks,

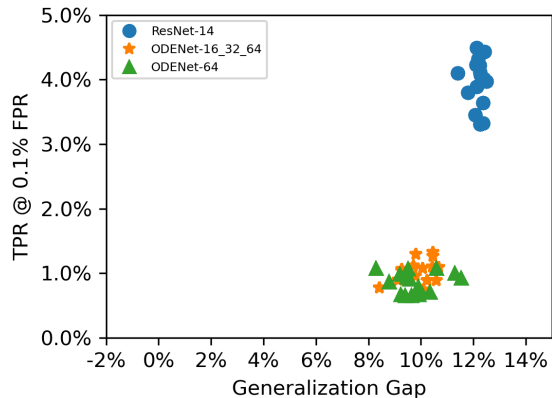


Figure 1. Membership risks and overfitting in CIFAR-10.

as shown in Table 2. In ResNets, the generalization gap is $>12\%$, and the TPR @ 0.1% FPR is 3–5%. In contrast, NODE models (ODENet-16_32_64 and -64), with 0.5–1.5% TPR @ 0.1% FPR, show the generalization gap in 8–12%. Please refer to Appendix for results in CIFAR-100.

3.4. Characterizing the Membership Risks

We now analyze factors that attribute to the membership inference risks. For this analysis, we use LiRA, where NODEs demonstrate the largest reduction in their risk. We examine block-level configurations, such as the choice of ODE solvers, and model-level factors, including the number of ODE blocks and the type of differential equations used to model a system. Figure 2 summarizes our results.

Impact of a solver. In all our experiments, we use Euler’s method as the default solver; but, other popular choices exist in the literature. We therefore analyze how the choice of solver impacts the membership risks of NODEs. We train and test the same NODEs with two other solvers: a fixed-step solver, Runge–Kutta (RK4) and an adaptive-step solver, Dormand–Prince (Dopri5).

The leftmost figure illustrates the success rate of LiRA on NODEs trained and tested with three different solvers. Overall, we observe a marginal difference in attack success across these models. In both CIFAR-10 and CIFAR-100 (shown in Appendix), the TPR remains 0.7–1.0% and 3.0–3.7% @ 0.1% FPR, respectively. Upon closer examination, Euler and RK4 yield similar risks, while Dopri5 shows 0.3% lower TPR at the same FPR. We attribute this to Dopri5’s use of adaptive step-sizes. During the training of a NODE model with Dopri5, it stops processing of an input when the error rate becomes sufficiently small—within the predefined tolerance value. It acts as an early-stopping mechanism [5], preventing the model from becoming overconfident on specific training samples. RK4, by modeling data with higher-order polynomials, may achieve an increased training (and testing) accuracy. However, the ability to perform complex modeling can introduce a risk of overfitting to specific training samples, which can also increase membership inference risks. In CIFAR-100, a more complex task than CIFAR-10,

we observe 0.3% and 1.0% higher TPR at 0.1% and 1% FPR, respectively, compared to the model using Euler.

Impact of the number of ODE blocks. Our NODEs replace a group of residual blocks with an ODE block, a configuration chosen for its comparable accuracy to ResNet models. One can also increase the number of ODE blocks further. We hypothesize that, because additional ODE blocks enhance the model’s ability to represent complex systems, this may lead to an increase in membership risks.

The middle figure compares the membership risks of NODEs as the number of ODE blocks increases from 1 to 3. We find that adding more ODE blocks leads to higher membership risks, likely due to the increased number of parameters, which raises the likelihood of *overfitting*. However, this increase does not yield significant performance gains, suggesting that simply adding more ODE blocks is not an effective strategy for improving the performance.

Non-stochastic NODE variants. In §2.1, we review NODE variants designed to enhance expressivity and stability, ultimately improving generalization. We examine whether these benefits come with a reduction in membership risks. We evaluate ANODE [16], SONODE [21] and HBNODE [18]. We select ODENet-64 as our baseline model because it is composed of a single ODE block, making it easy to extend to NODE variants. We implement SONODE and HBNODE using an ODE block identical to that in ODENet-64. We augment ODENet-64 with an additional 16 and 64 dimensions (ANODE). These variants are expected to enhance the model’s generalization capabilities, allowing us to assess the impact of better system modeling on membership risks.

The rightmost figure compares the membership risks of these models with those of the baseline ODENet-64 model. We first observe that NODE variants, except for the HBNODE model, achieves higher test accuracy (84.6–86.5%) than the baseline (84.4%). SONODE performs the best with 86.5%, followed by ANODE (+64) at 85.1% and ANODE (+16) at 84.6%. But HBNODE achieves 82.1%. Interestingly, we find that *all the NODE variants are less vulnerable* to LiRA. SONODE, ANODE (+64), ANODE (+16), and HBNODE achieve TPRs of 0.44%, 0.35%, 0.24%, and 0.24% at 0.1% FPR, respectively, compared to ODENet-64 with a TPR of 0.86% at 0.1% FPR. We attribute this to the reduced overfitting shown by NODE variants. The differences between training and testing accuracy are 5.9%, 4.0%, 3.0%, and 2.8% for SONODE, ANODE (+64), ANODE (+16), and HBNODE, respectively, compared to 9.7% gap in ODENet-64. However, for HBNODE, there is a possibility that the lower risk is attributed to the lack of generalization. Modeling NODEs with momentum (HBNODE) enhances the stability, but does not increase a model’s capacity. In our evaluation, the training accuracy of HBNODE is 84.9%, 2.8–7% lower than that of the other variants.

4. NSDEs Are DP-Learners

In the previous section, we demonstrated that NODEs and their non-stochastic variants are still vulnerable to membership inference attacks. We now shift our focus to the

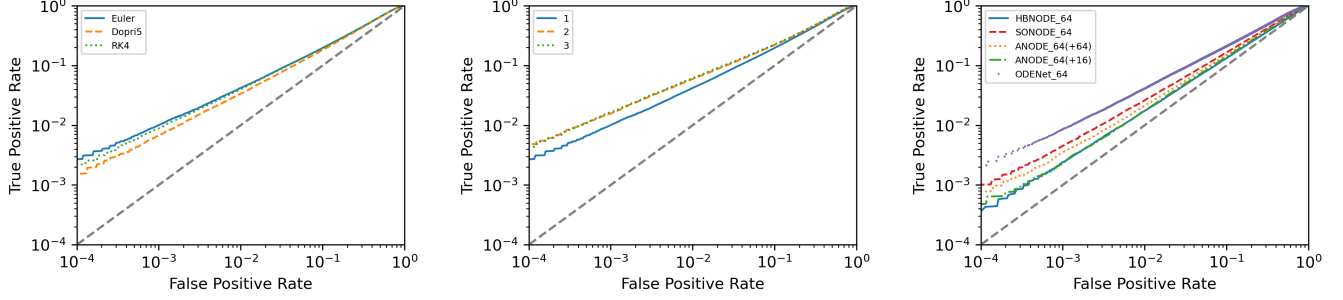


Figure 2. **Characterization of membership risks in NODEs with different configurations.** We vary the choice of ODE solvers (left), the number of ODE blocks (middle), and the equations used for modeling a system (right). We show the results in CIFAR-10 against LiRA [6], the strongest membership inference attack. Please refer to Appendix for details and results in CIFAR-100.

stochastic variants of NODEs, particularly neural stochastic differential equations (NSDEs) [32]. In NSDEs, which contain “drift” and “diffusion” terms, stochasticity arises from the *randomness in the diffusion term*, typically modeled as white or colored Gaussian noise. We hypothesize that this diffusion term leads NSDEs to act as a differentially-private (DP) mechanism [33], preserving the privacy of its inputs along its evolution. Here we first formally show that NSDEs are DP-learners. Because of the diffusion term, those models learn “differentially-private” systems of ODEs, achieving privacy without the need of additional mechanisms, such as DP-SGD [23], which alters the training process. Next in §5, we empirically assess the membership risks of NSDEs in comparison to non-stochastic NODE variants and “private” feedforward models trained with DP-SGD.

4.1. Theoretical Analysis

NSDEs model the dynamics of system states as:

$$d\mathbf{h} = \mathbf{f}(\mathbf{h}, t) dt + \mathbf{G}(\mathbf{h}, t) d\mathbf{B}_t,$$

in terms of a drift function $\mathbf{f} : \Omega \rightarrow \mathbb{R}^n$ and a diffusion term $\mathbf{G} : \Omega \rightarrow \mathbb{R}^{n \times n}$, where the explicit dependence on parameters Θ has been dropped for notational convenience. Our privacy bounds will make use of the *sensitivity* of a function $g : \Omega \rightarrow \mathbb{R}^n$ (c.f. [33]):

$$S_g = \max_{|\mathbf{h}-\mathbf{h}'| \leq 1} |g(\mathbf{h}) - g(\mathbf{h}')|.$$

Here, we adopt the following natural assumptions from the work by Liu *et al.* [32], which guarantees the well-posedness of the SDE formulation under consideration.

Assumption 1 (Sublinear Growth). \mathbf{f} and \mathbf{G} grow at most linearly, i.e., there exists a constant $c > 0$ such that $|\mathbf{f}(\mathbf{h}, t)| + |\mathbf{G}(\mathbf{h}, t)| \leq c(1 + |\mathbf{h}|)$ for all $\mathbf{h} \in \Omega$ and $t \geq 0$.

Assumption 2 (Lipschitz Continuity). \mathbf{f} and \mathbf{G} are L -Lipschitz, i.e., there exists a constant $L > 0$ such that $|\mathbf{f}(\mathbf{h}, t) - \mathbf{f}(\mathbf{h}', t)| + |\mathbf{G}(\mathbf{h}, t) - \mathbf{G}(\mathbf{h}', t)| \leq L|\mathbf{h} - \mathbf{h}'|$ for all $\mathbf{h}, \mathbf{h}' \in \Omega$ and $t \geq 0$.

With these conditions in place, the following theorem establishes the differential privacy of the SDE mechanism.

Theorem 1 (SDEs Are Differentially-Private). Suppose σ , $T > 0$ and $\mathbf{f}(\mathbf{h}, t) : \Omega \rightarrow \mathbb{R}^n$ is Lipschitz-continuous with constant L_f . Consider the well-posed SDE:

$$d\mathbf{h} = \mathbf{f}(\mathbf{h}, t) dt + \frac{\sigma}{\sqrt{T}} d\mathbf{B}_t.$$

For any privacy budget $0 < \epsilon < 1$ and failure probability $\delta > 0$, the mechanism $\mathcal{M}(\mathbf{h}) = \mathbf{h}(T)$, defined by the flow map of the SDE at time T , is (ϵ, δ) -differentially private, provided that $\sigma \geq \sqrt{2 \ln(1.25/\delta)}(TL_f/\epsilon)^2$.

Proof. Recall that the Wiener increment $d\mathbf{B}_t$ satisfies $\int_s^t d\mathbf{B}_\tau = \mathbf{B}_t - \mathbf{B}_s \sim \mathcal{N}(\mathbf{0}, (t-s)\mathbf{I})$. It follows that the solution to the hypothesized SDE can be formally expressed as:

$$\mathbf{h}(T) = \int_0^T \mathbf{f}(\mathbf{h}, t) dt + \frac{\sigma}{\sqrt{T}} \int_0^T d\mathbf{B}_t := \mathbf{F}(\mathbf{h}) + \mathbf{B}_T,$$

where $\mathbf{B}_T \sim \mathcal{N}(\mathbf{0}, \sigma^2 \mathbf{I})$ represents additive Gaussian noise and \mathbf{F} denotes deterministic part of the SDE evolution. Proposition 1 in Appendix shows that this mechanism obeys (ϵ, δ) -differential privacy whenever $\epsilon < 1$ and $\sigma \geq \sqrt{2 \ln(1.25/\delta)}(S_{\mathbf{F}}/\epsilon)$. The claimed bound on the variance σ follows since the sensitivity $S_{\mathbf{F}}$ is bounded above due to Lipschitz continuity in \mathbf{f} :

$$\begin{aligned} S_{\mathbf{F}} &= \max_{|\mathbf{h}-\mathbf{h}'| \leq 1} |\mathbf{F}(\mathbf{h}) - \mathbf{F}(\mathbf{h}')| \\ &\leq \max_{|\mathbf{h}-\mathbf{h}'| \leq 1} \int_0^T |\mathbf{f}(\mathbf{h}, t) - \mathbf{f}(\mathbf{h}', t)| dt \\ &\leq \max_{|\mathbf{h}-\mathbf{h}'| \leq 1} \int_0^T L_f |\mathbf{h} - \mathbf{h}'| dt \leq TL_f. \quad \square \end{aligned}$$

Remark 1. Importantly, Theorem 1, while stated continuous time, also holds in discrete time—for instance, with the Euler–Maruyama integration method—as long as the function $\mathbf{F}(\mathbf{h}) = \int_0^T \mathbf{f}(\mathbf{h}, t) dt + \epsilon(\mathbf{h})$ appropriately accounts for the quadrature error introduced by this discretization. Assuming Lipschitz continuity in the error term ϵ , the claimed variance bound holds with TL_f replaced by $TL_f + L_\epsilon \geq S_{\mathbf{F}}$. While this quadrature error may affect

2. Note that ϵ and δ here are different from those used in §2.3.

solution accuracy, it does not affect the privacy guarantee, since each Euler sub-step adds a statistically independent fraction of the total required Gaussian noise, and therefore the total amount of noise added is equivalent even if the exact and approximate Gaussian contributions differ. Notably, only the approximate output $\mathbf{h}(T)$ at the final time is private and appropriate for release in this case.

Theorem 1 provides an additive noise threshold which guarantees differential privacy in the NSDE forward pass. Although Theorem 1 is stated for a constant diffusion term $\mathbf{G}(\mathbf{h}, t) = (\sigma/\sqrt{T})\mathbf{I}$, it continues to hold for a general Lipschitz-continuous, at most linear $\mathbf{G}(\mathbf{h}, t)$, provided the Gaussian random variable $\int_0^T \mathbf{G}(\mathbf{h}, t) dt$ satisfies the stated variance bound for each \mathbf{h} . Moreover, since computing gradients of the NSDE model with respect to its parameters accesses the private input data only through the SDE output $\mathbf{h}(T)$, the following Corollary demonstrating that differential privacy extends to the entire NSDE training process.

Corollary 1 (NSDE Training is Differentially Private). Consider target privacy parameters $0 < \epsilon' < 1$ and $\delta' > 0$ with a maximum iteration count of K . Then, NSDE training of the drift \mathbf{f} in Theorem 1 will be $(\epsilon', K\delta + \delta')$ -differentially private as long as the variance satisfies $\sigma \geq 4\sqrt{K \ln(1.25/\delta) \ln(1/\delta')}(TL/\epsilon')$. Here, $\delta > 0$ is arbitrary and $L = \max_{\mathbf{f}} L_{\mathbf{f}}$ denotes the maximum Lipschitz constant attainable by \mathbf{f} during training.

Proof. Note that, by the parallel composition principle, mini-batching into disjoint subsets at each iteration does not increase the total privacy leakage, as each individual’s data in the state \mathbf{h} is accessed only once by the SDE mechanism. Similarly, the composition of the NSDE output with a downstream classifier does not degrade (ϵ, δ) -differential privacy guarantees, as these guarantees are immune to post-processing by construction. Consequently, the total privacy leakage in NSDE training is directly proportional to the number of training iterations K , corresponding to the number of accesses to the private input \mathbf{h} . The result follows from the Strong Composition Theorem in Dwork *et al.* [44] [Theorem 3.20, Corollary 3.21], in combination with the variance bound established in Theorem 1. \square

Remark 2. Note that determining the Lipschitz constant L in Corollary 1 is most easily accomplished by restricting the NSDE architecture to guarantee a particular Lipschitz bound, see, e.g., [45]. Moreover, it should be noted that the privacy guarantees presented here are not necessarily tight in every case and may be improved with more sophisticated privacy accounting mechanisms, such as those in [23], [46].

Corollary 1 guarantees the privacy of NSDE training provided that the diffusion term is constructed to add enough stochastic noise along NSDE solution trajectories. This has the remarkable advantage of privatizing learning without requiring direct intervention in the training process: the network dynamics are already private, therefore no further privacy-preserving modifications are required during the backward pass. In contrast, DP-SGD must use inexact

gradient information in order to retain privacy, which can potentially hinder the training process.

5. Empirical Evaluation

We now empirically evaluate the effectiveness of NSDEs, as a DP-learner, in mitigating membership inference attacks. We run our evaluation on the CIFAR-10 and CIFAR-100 datasets, where membership inference attacks are shown to be most effective. Our NSDE models (**SDENet**) adopt architectural configurations similar to ODENet, comprising three groups of ODEBlocks with 16, 32, and 64 dimensional filters, respectively, widened by a factor of 2. In SDENet, stochasticity is introduced by employing an SDE solver within the ODEBlocks, utilizing a stochastic fourth-order Runge-Kutta (RK4) integration method. SDENet also incorporates a hyper-parameter (σ) to control noise intensity, influenced by factors such as time, step size, and the desired level of stochasticity.

5.1. Effectiveness of NSDEs

We conduct three comparisons: (1) NSDEs with ResNet-14 to assess whether stochasticity reduces the empirical membership risks. (2) NSDEs with heuristic defenses discussed in §2, which lack provable privacy guarantees. (3) NSDEs with “private” ResNet-14 trained with DP-SGD. In (2), we consider four defenses studied in prior work [24], [36], [37], [47]: ℓ^1/ℓ^2 -regularization, MMD-Mixup, and MemGuard. For ℓ^1/ℓ^2 -regularization, we set the penalty parameter λ to 10^{-5} . We use the most robust version of MemGuard as described in Choquette *et al.* [48], which allows for arbitrary adjustments to the confidence vector while preserving the model’s predicted label. For MMD-Mixup, we adopt the implementation from the study by Li *et al.* [37], and set the penalty parameter λ to 5×10^{-4} . In (3), when training with DP-SGD, we set the privacy budget ϵ to 8, a common choice for CIFAR-10 and 100 in prior work [47]. We use the popular Opacus library³ to implement privacy accounting in NSDE training and to compute the total privacy leakage (ϵ).

(1) Mitigating membership inference attacks. We first compare the membership inference risks of NSDEs and NODEs against six existing attacks. Table 3 shows our results. Across four evaluation metrics, NSDE reduce attack success by 4–10 \times compared to NODEs. Particularly against the LiRA attack, NSDEs achieve a TPR of 0.14–1.24% at both 0.1% and 1% FPRs, while NODEs exhibit a higher TPR of 1.0–4.22% under the same conditions (FPRs).

(2) Comparing with heuristic defenses. Figure 3 summarizes our results against LiRA, the membership inference attack where we observe the most significant reduction in attack success. Overall, we first demonstrate that *NSDEs effectively mitigate membership inference risks*. Compared to ResNet-14, a feedforward model that yields 3.96–10.57%

3. Opacus: <https://github.com/pytorch/opacus/>

TABLE 3. CONTRASTING MEMBERSHIP INFERENCE RISKS OF NSDES AND NODES. WE EVALUATE BOTH MODELS WITH SIX ATTACKS.

Model	Method	TPR @ 0.1% FPR				TPR @ 1% FPR				AUC				Inference acc.			
		F-M	C-10	C-100	T-I	F-M	C-10	C-100	T-I	F-M	C-10	C-100	T-I	F-M	C-10	C-100	T-I
NODE	Yeom et al. [3]	0.00%	0.00%	0.01%	0.09%	0.06%	0.00%	0.71%	1.12%	0.518	0.558	0.701	0.645	52.55%	56.59%	70.75%	61.23%
	Shokri et al. [4]	0.09%	0.04%	0.04%	0.10%	0.90%	0.43%	0.37%	1.01%	0.493	0.448	0.398	0.502	50.15%	50.01%	50.00%	50.21%
	Song and Mittal [38]	0.00%	0.00%	0.15%	0.12%	0.53%	0.00%	1.66%	1.19%	0.507	0.529	0.498	0.500	50.98%	54.22%	52.48%	50.45%
	Watson et al. [34]	0.00%	0.00%	0.01%	0.12%	0.04%	0.00%	0.71%	1.17%	0.517	0.558	0.701	0.542	52.04%	56.69%	70.75%	53.24%
	Carlini et al. [6]	0.19%	1.01%	3.30%	0.24%	1.48%	4.22%	12.11%	1.74%	0.529	0.616	0.782	0.543	52.81%	57.65%	72.88%	52.95%
Zarifzadeh et al. [35]	0.67%	1.93%	5.41%	0.26%	3.16%	6.57%	17.58%	2.04%	0.523	0.592	0.797	0.570	53.05%	58.17%	73.37%	55.04%	
SDENet ($\sigma=2$)	Yeom et al. [3]	0.00%	0.02%	0.05%	0.11%	0.06%	0.92%	1.09%	1.13%	0.526	0.525	0.588	0.557	54.17%	52.44%	56.96%	54.72%
	Shokri et al. [4]	0.09%	0.09%	0.08%	0.11%	0.94%	0.86%	0.85%	1.03%	0.498	0.484	0.473	0.502	50.14%	50.04%	50.00%	50.40%
	Song and Mittal [38]	0.00%	0.00%	0.12%	0.12%	0.18%	0.20%	1.34%	1.05%	0.497	0.509	0.498	0.499	50.12%	50.95%	50.84%	50.12%
	Watson et al. [34]	0.01%	0.02%	0.05%	0.11%	0.18%	0.91%	1.09%	1.12%	0.515	0.525	0.588	0.519	51.02%	52.44%	52.44%	51.91%
	Carlini et al. [6]	0.10%	0.14%	0.43%	0.12%	0.97%	1.24%	3.00%	1.14%	0.500	0.625	0.612	0.509	50.01%	51.89%	57.64%	50.77%
Zarifzadeh et al. [35]	0.27%	0.38%	0.83%	0.16%	1.82%	2.39%	4.60%	1.45%	0.527	0.554	0.646	0.535	51.12%	54.11%	59.25%	52.67%	

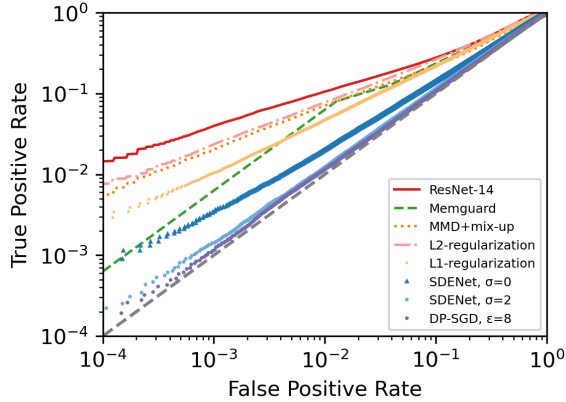


Figure 3. Comparing the effectiveness of different defenses, in CIFAR-10. We use LiRA to assess their membership risks. All defenses, except for SDENets, are applied to ResNet-14.

TPR at both 0.1% and 1% FPR, NSDEs with $\sigma = 2$ achieve approximately two orders of magnitude lower TPRs (0.14–1.24%). We also find that NSDEs significantly outperform heuristic defenses in reducing membership inference risks. Compared to the four empirical defenses— ℓ^1/ℓ^2 -regularization, MMD-Mixup and MemGuard—NSDEs with $\sigma=2$ achieves 2–8 \times lower TPRs at 0.1–1% FPRs.

(3) Comparison with private models constructed via DP-SGD. NSDEs match the effectiveness of ResNet-14 trained with DP-SGD at $\epsilon = 8$. It is interesting to observe that even the non-private variant of NSDEs (i.e., $\sigma=0$) achieve lower TPRs than these defended models. NSDEs with $\sigma=0$ achieve a test accuracy of 83.9%, which, though slightly lower than ResNet-14’s 86.0%, significantly narrows the generalization gap from 12.2% to 5.2%. This narrowing leads to a markedly lower TPR at 0.1% FPR: 0.4% for NSDEs versus 4.0% for ResNet-14. NSDEs with $\sigma = 2$ attain a test accuracy of 81.9% and nearly eliminate the generalization gap (-0.02%), further reducing the TPR to 0.1% at 0.1% FPR. Compared to ℓ^1 and ℓ^2 -regularization, NSDEs with $\sigma = 2$ not only provide a modest reduction in test accuracy by 4.6%–4.7%, but also enhance defenses, achieving a TPR at 0.1% FPR of 0.14% versus 1.1% for ℓ^1 and 2.4% for ℓ^2 . While DP-SGD with $\epsilon = 8$ realizes a smallest generalization gap, it significantly compromises test accuracy, dropping 7.5–9.5% compared to NSDEs ($\sigma = 0$

and $\sigma=2$). Consequently, NSDEs demonstrates an improved overall performance in terms of both model training (higher test accuracy) and defense against membership inference attacks, making it a more balanced and practical approach. Please refer to Appendix for further details.

Moreover, to understand where the resilience of NSDEs against these attacks comes, we compare the generalization gap in Table 4. In NODEs, the gap is 9.9–29.89% for CIFAR-10 and CIFAR-100, while in NSDEs, it is 0.0–5.9%. This result implies that *the reduction in membership risks in NSDEs is partly due to a significant reduction in overfitting.*

TABLE 4. GENERALIZATION GAP, MEASURED FOR BOTH NODE MODELS AND NSDE MODELS ACROSS FOUR BENCHMARK DATASETS.

Task	F-M		C-10		C-100		T-I	
Model	NODE	NSDE	NODE	NSDE	NODE	NSDE	NODE	NSDE
Train	95.5%	96.2%	94.3%	81.9%	82.1%	56.5%	55.9%	39.9%
Test	90.0%	89.2%	84.4%	81.9%	52.2%	50.6%	40.5%	38.1%
Δ	5.5%	7.0%	9.9%	0.0%	29.9%	5.9%	15.4%	1.8%

5.2. In-depth Analysis of Privacy of NSDEs

We next analyze the privacy guarantee (ϵ) provided by NSDEs. Because we theoretically show that NSDEs are DP-learners (with the privacy guarantee equivalent to those of DP-SGD), it is important to understand empirically whether their privacy interactions behave similarly to observations from prior work [49]. We first compare the privacy leakage of NSDEs with the worst-case leakage bound established by DP-SGD. We also examine the impact of privacy hyperparameters—such as δ and the choice of privacy accounting algorithms—on the guarantee ϵ and the model utility.

Comparison to the theoretical DP-SGD bound. Figure 5 compares the empirical success of LiRA against NSDEs with $\sigma = 2$ to the theoretical upper-bound of DP-SGD (when $\epsilon = 1$). Note that training NSDEs with $\sigma = 2$ while targeting $\epsilon = 1$ completely destroys the model utility, making any meaningful LiRA success unattainable. To maintain utility, we target $\epsilon = 8$ in our experiments with NSDEs. This does not compromise the generality of our results, because even against NSDEs with weaker privacy guarantees, the empirical attack (LiRA) does not exceed the DP-SGD bound. We first observe that the attack success of LiRA on

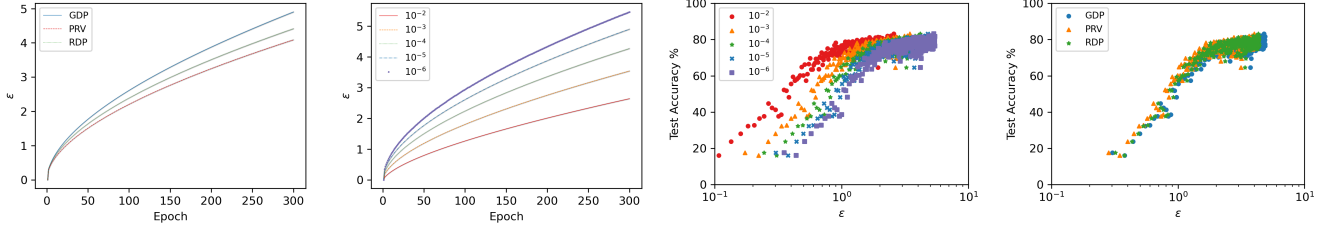


Figure 4. **Impact of privacy hyper-parameters on NSDE training** in CIFAR-10. We analyze the total privacy leakage (ϵ) in the left two plots and the privacy-utility tradeoff in the right two plots, while varying key hyper-parameters.

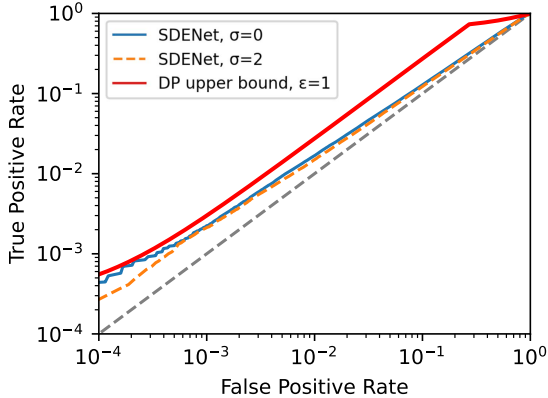


Figure 5. **Comparing the empirical membership risks of NSDEs with the theoretical bound by DP-SGD.** We use LiRA to measure the membership risks and the theoretical bound when $\epsilon=1$ is computed by the method presented in [6]. NSDE with $\sigma=2$ is used to compare, and that with $\sigma=0$ is its non-private version. The shaded areas give the 68% (darker) and 95% (lighter) confidence intervals.

NSDEs with $\sigma=2$ remains within the worst-case leakage bound established by DP-SGD. However, when the diffusion mechanism is removed ($\sigma=0$), LiRA’s attack success often goes beyond the DP-SGD bound, especially at lower FPR regions (e.g., at 0.1–1% FPR), highlighting the absence of formal privacy guarantees in non-stochastic variants.

Privacy leakage ϵ over training. The left two plots in Figure 4 illustrate the total privacy leakage (ϵ) during NSDE training. As expected, both plots show that privacy leakage increases with training epochs. However, the growth rate decreases over time—consistent with empirical findings from prior work on training models with DP-SGD [23].

The leftmost plot compares privacy leakage estimates produced by three different accounting methods: Gaussian Differential Privacy (GDP), Renyi Differential Privacy (RDP), and Privacy loss Random Variables (PRVs). Among them, GDP consistently yield higher estimates of privacy leakage compared to the other two methods. This is partly because GDP relies on Gaussian approximations, which often deviate from the true privacy loss distribution. In contrast, precise accounting methods like RDP or PRVs, which enable tracking the exact or near-exact cumulative privacy loss, provide tighter privacy bounds. Moreover, because privacy loss accumulates over time, the discrepancy between GDP and the more precise methods progressively

widens as the number of training epochs increases.

The second plot from the left shows the total privacy leakage computed using the GDP accountant across varying δ values, from 1×10^{-2} to 1×10^{-6} . As δ increases, so does the total privacy leakage (ϵ), consistent with theoretical expectations. This is because δ represents the probability of rare but catastrophic privacy failures (e.g., data leakage from physical breaches). Allowing for a higher δ weakens the privacy guarantee by tolerating a greater failure risk.

Privacy-utility trade-off. The right two plots in Figure 4 illustrate the test accuracy of NSDEs trained with different privacy budgets (ϵ). We record the test accuracy and privacy leakage at each training epoch for the 16 models used in our evaluation, and we plot them. The second figure from the right shows the trade-offs across different failure probabilities (δ). As δ increases, the test accuracy of NSDEs increases under the same privacy budget. This is because a larger δ permits a higher likelihood of privacy leakage. Surprisingly, NSDEs achieve a test accuracy of 80% with $\epsilon=2$ and $\delta=10^{-5}$ under GDP, which demonstrates their ability to maintain high utility even at relatively low privacy budgets. The rightmost plot demonstrates that all three accountants produce similar estimates of privacy leakage and test accuracy. However it is important to note the variability in test accuracy: even under the same privacy budget, e.g., $\epsilon=2$, test accuracy ranges from 65–82%. We attribute this variance to the factors like randomness introduced by the diffusion term or the training data stochasticity. In practice, to train NSDEs with high utility we may need to train the same model multiple times, as shown in prior work [47].

5.3. Impact of NSDE Configurations

We now turn our attention to the impact of NSDE configurations on their membership risks. In this analysis, we maintain consistent hyper-parameters that affect privacy accounting when varying, such as the number of training iterations, batch-size and learning rate. The only exception is the noise intensity (σ) which directly influences the total privacy leakage. We examine five configurations: the number of NSDE blocks n , the level of stochasticity k , the integration time interval T , the step-size $1/s$, and the noise intensity σ . It is important to note that the noise intensity depends on the first three variables, following the formulation $\frac{k}{\sqrt{T/s}}$.

The number of SDE blocks (n). We investigate the impact of adding more SDE blocks on privacy. Due to the

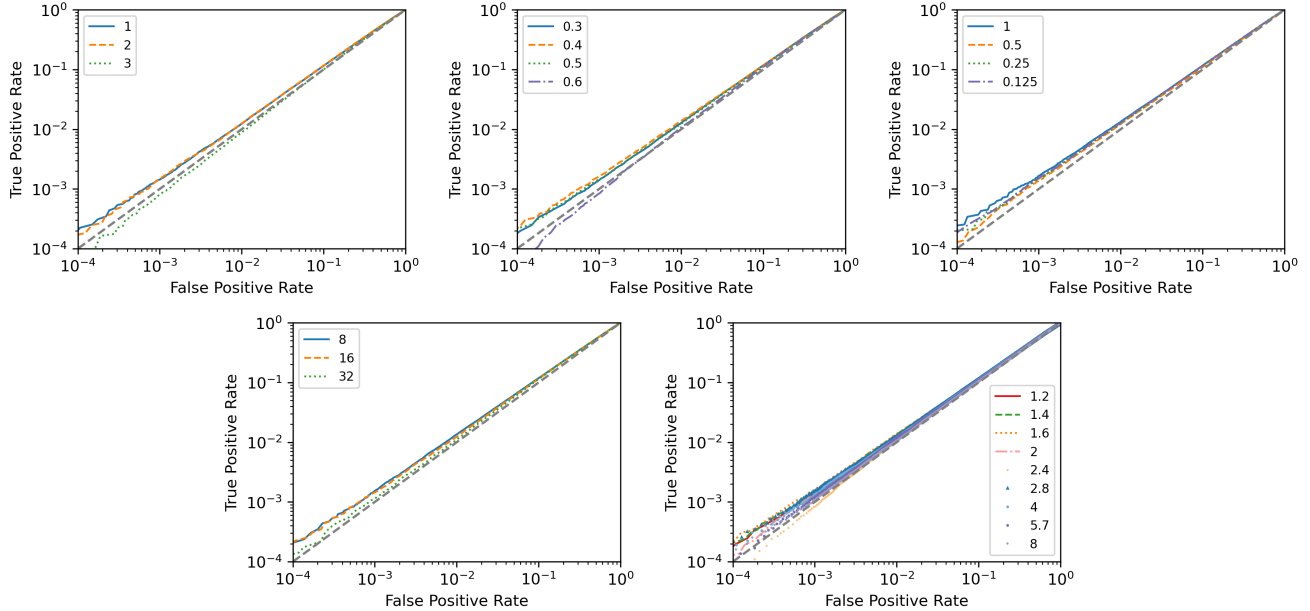


Figure 6. **Membership risks of NSDEs trained with different configurations.** (Top row, left to right) We illustrate the impact of the number of blocks (n), the level of stochasticity (k), and the step-size (s). (Bottom row, left to right) We show the impact of the integration time T and the noise intensity σ . We use LiRA to assess the membership risks. The results are in CIFAR-10.

post-processing property of DP, connecting multiple SDE blocks sequentially—each with the privacy guarantee ε —still results in an overall privacy leakage bounded by ε . However, we expect that the diffusion terms in these blocks will introduce random noise multiple times, leading to a substantial decrease in model utility. We vary $n \in \{1, 2, 3\}$.

The top-left plot in Figure 6 illustrates our results. Membership risks associated with NSDE models are consistent when $n=1$ or $n=2$. But employing three SDE blocks reduces the risks by a factor of 2, as measured by TPRs at 0.1–1% FPR. We attribute this reduction to poor generalization when $n=3$. For instance, in CIFAR-10, while NSDEs with $n \in \{1, 2\}$ achieve test accuracy of 81.9–82.4%, models with $n=3$ show significantly lower test accuracy of 74.4%. Interestingly, unlike NODEs, augmenting the number of SDE blocks in NSDEs leads to a corresponding reduction in membership risks.

The level of stochasticity (k) directly increases the novel intensity (σ) for the Gaussian diffusion term, following the formula $\sigma = \frac{k}{\sqrt{T/s}}$. Increasing k adds more noise to the modeling dynamics, and therefore, a reduction in membership risks. We vary k across $\{0.3, 0.4, 0.5, 0.6\}$, with a default value of 0.5 for all our experiments.

The top-middle plot illustrates our findings. We show that NSDEs with varying k values effectively mitigate membership risks, as measured by LiRA. With k values up to 0.5, NSDEs exhibit the same level of effectiveness. But when k reaches to 0.6, it completely mitigates the membership risks, bringing the ROC curve below that of a random classifier (a diagonal line). We also examine how each choice of k affects model performance. Increasing the level of stochasticity results in a decrease in model utility. On CIFAR-10, the test

accuracy drops from 82.6% to 57.1% as k increases from 0.3 to 0.6. This result implies that the state-of-the-art attack (LiRA) is yet weak so that one can completely mitigate with k that does not significantly degrade model utility.

The integration time interval T . We evaluate the impact of varying integration time intervals by adjusting T and measuring its impact on membership risks. We set T across $\{0.125, 0.25, 0.5, 1\}$, with the default value of $T=1$ used in all our experiments.

The top-right plot in the same figure illustrates our findings. Overall, we find no significant interaction between the integration time interval (T) and membership risks. All NSDE models consistently show low membership risks. But theoretically, decreasing T will increase the noise intensity (σ), leading to a smaller privacy leakage (ε) with reduced model utility and membership risks.

The step-size ($1/s$), which controls the granularity at which the integration over time T is computed. The increase in s results in a model less capable of learning details of dynamics in the training data. We vary s across $\{8, 16, 32\}$, with the default value of 16.

The bottom-left plot in Figure 6 summarizes our findings. Overall, we observe only marginal variations in membership risks caused by changes in step size ($1/s$). On CIFAR-10, the membership risks observed at $s=8$ or 16 are comparable. However, we find a reduction of the risks with $s=32$, likely because the model lacks learning detailed dynamics from the training data. Our analysis indicates that this reduction comes at the cost of accuracy. A step size of 32 limits NSDEs effectiveness in modeling underlying dynamics, and in consequence, they experience substantial performance degradation. NSDEs at this step size achieve

an average accuracy of 35.9%, which is 46.5–46.1% lower than that achieved with s of 8 or 16.

The noise intensity (σ). We finally examine how the noise intensity σ affect membership risks, though this parameter being influenced by our choice of σ, T and s . To evaluate this, we collect results across all combinations of these three configurations from our previous experiments. This results in unique σ values of $\{1.2, 1.4, 1.6, 2.0, 2.8, 4.0, 5.7, 8.0\}$, with duplicates removed. We use LiRA to quantify (empirical) membership risks.

The bottom-right plot illustrates our results. Overall, we observe that all the noise intensity values we examine effectively mitigate membership risks, consistent with prior work [6], which shows that even the strongest membership inference attacks can be easily countered by a weak privacy guarantee provided by DP-SGD. We also demonstrate that as the noise intensity gets stronger, NSDE’s effectiveness increases. However, it is important how we configure the noise intensity. For instance, setting a lower noise intensity, such as 1.6, by employing a larger step-size (e.g., 32), may appear to reduce membership risks in the figure. But this reduction is primarily due to a substantial drop in model utility, as shown in our analysis of different step-sizes.

5.4. NSDE as a Drop-in Replacement Module

All our evaluations so far assume that a defender trains NSDE models from scratch. This approach often requires more computational resources than expected, and could potentially face pushback, especially when well-performing pre-trained models are available. To address this issue, we present an efficient *replace-then-finetune* strategy. Instead of training NSDEs from scratch, we propose *replacing* the last few layers of an existing pre-trained model with an NSDE block and *then finetune*. This approach reduces computational demands by re-using the majority of pre-trained parameters, as it requires fewer training iterations, while also benefiting from NSDEs’ privacy advantages (based on DP’s composition theorem). It also potentially improves model utility, as fine-tuning leverages the features (i.e., the latent representations/activations obtained at the penultimate layer), a strategy demonstrated to be effective in prior work on training models with DP-SGD [50]. In the following, we present results on CIFAR-10. We refer the readers to Appendix for results on other datasets.

Impact on privacy. Figure 7 demonstrates the effectiveness of the replace-then-finetune strategy. When the last group of the final residual block is replaced with an NSDE block, membership risks are reduced by more than an order of magnitude, particularly in low FPR regions, compared to ResNet-14. However, when compared to the NSDE models trained from scratch, membership risks are higher. This does not imply a difference in the privacy guarantees (ϵ) between the two models. Their guarantees remain the same due to the post-processing property.⁴ LiRA may hit the worst-case

4. Note that the last NSDE block is randomly initialized and fine-tuned.

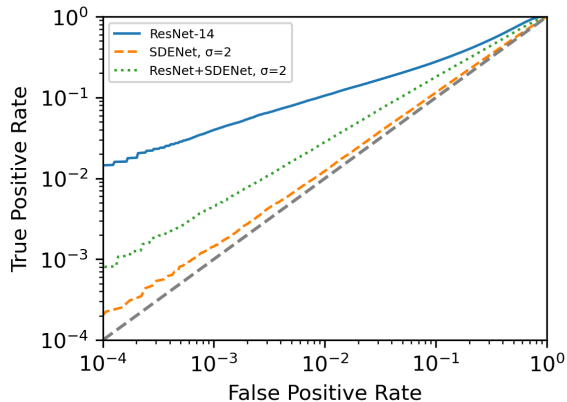


Figure 7. **Effectiveness of *replace-and-finetune* strategy.** We replace the last residual block of ResNet14 with a NSDE block and then finetune the adapted model on CIFAR-10.

privacy leakage against the replace-then-finetuned models, as indicated by the bound shown in Figure 5.

Impact on model utility. We also observe that the test accuracy of the replace-then-finetuned models is 84.0%, a modest decrease from the 86.0% achieved by ResNet-14. However, this reduction is comparatively smaller than that observed in NSDEs trained from scratch, which achieves a test accuracy of 81.9%. We emphasize that this approach also offers potentially reductions in the computational demands of NSDE training. Notably, we observe that test accuracy stabilizes after 150 epochs, which is half the total number of epochs we use for training NSDEs. As shown in our theoretical analysis in §4.1, a reduction in the number of training iterations (K) also decreases the total privacy leakage of the trained models. Our results demonstrate the effectiveness of the replace-then-finetune strategy in reducing membership inference risks while maintaining high utility and reducing computational overhead.

6. Related Work

Privacy attacks on machine learning. Membership inference attacks—where an adversary, given a particular instance, attempts to infer whether it was part of a model’s training data—represent a worst-case form of privacy leakage and have been widely studied as a key mechanism for privacy auditing in machine learning. However, other types of privacy attacks have also been explored in the literature.

Fredrikson *et al.* [51] introduced the concept of *model inversion*, a class of reconstruction attacks aimed at reverse-engineering training samples or recovering sensitive information in the training data that has not exposed to public. Initial work [51] focused on attacks targeting linear models, while subsequent work [52], [53] extended these attacks to non-linear models, including decision trees and neural networks. In particular, these attacks against neural networks typically involve iterative gradient-based optimization to refine inputs until they resemble the original training data.

When a model inversion is used to infer sensitive attributes—such as gender or race—of specific training in-

stances, it is referred to as *attribute inference attacks* [3]. These attacks exploit query access to a target model to extract unknown attributes from partially observed training records. Various attack methodologies [3], [51], [54] have been proposed, and attribute inference has been exploited across domains, such as social media [55], [56], [57], [58], [59], [60] or recommender systems [61], [62].

The recent emergence of advanced neural networks, such as language models, diffusion models, and differential equation-based networks like NODEs, necessitates the adaptation and evaluation of existing privacy attacks on these models. While much attention has been given to language models and diffusion models, with prior studies [63], [64], [65] demonstrating their susceptibility to membership inference and model inversion (or data extraction) attacks, no prior work has systematically studied the privacy risks of differential equation-based neural networks such as NODEs and NSDEs. Our work addresses this gap by presenting the first study on understanding and mitigating the membership risks associated with differential equation-based models.

Robustness of differential equation-based networks. In the existing literature, the security and privacy aspects of NODEs and NSDEs have mainly focused on countering *adversarial examples* [66] and ensuring the stability of learned dynamics. Time-invariant steady NODEs (TisODEs) [67], for instance, empirically demonstrated that NODEs are more resilient to random Gaussian noise and adversarial examples than traditional convolutional neural networks. TisODEs introduced a steady-state regularizer that minimizes the deviation of hidden states $\mathbf{h}(t)$ beyond a terminal time T (i.e., steady-state after T), effectively encouraging the network to learn stable dynamics. Similarly, Kang *et al.* [68] proposed guiding trajectory evolution toward Lyapunov-stable equilibrium points, enabling NODEs to extract features around stable attractors. This approach led to improved robustness against adversarial examples. The idea has been further extended to non-autonomous dynamical systems, guiding trajectories to asymptotically stable equilibrium points [69]. In [70], robustness analysis has also been extended to high-dimensional NODEs using graph-based verification tools.

Other techniques to improve NODE robustness include using skew-symmetric ODE blocks [71] and integrating Gaussian process [72], both of which empirically enhance robustness. Though not explicitly designed for adversarial robustness, some efforts contribute similarly by regularizing NODE dynamics. Kinetic and Jacobian norm regularizers [73], along with higher-order derivative regularizers [74], have been proposed to enforce smoothness in NODE dynamics and have been shown to be effective. The method proposed in STEER [75] mitigates the learning of stiff ODEs by randomizing the terminal times during training.

In contrast, there are only handful of works that have investigated security and privacy aspects of NSDEs. A few notable works include Jia *et al.* [76], who demonstrated that attributions generated from NSDEs are less noisy, visually sharper, and quantitatively more robust than those computed from deterministic NODEs. Liu *et al.* [32] also showed

formally and empirically that NSDEs improve robustness against adversarial examples. More broadly, NSDEs have been widely adopted as a tool to estimate uncertainty [77] and generative modeling [30].

7. Conclusion

This work studies the privacy implications of emerging neural networks, specifically NODEs, through the lens of membership inference attacks. To our knowledge, this is the first work that conducts a *comprehensive analysis* of the membership risks associated with NODEs. Our key findings are: (1) NODEs are twice as resilient to existing membership inference attacks compared to conventional feedforward models like ResNets, while maintaining comparable accuracy. (2) This privacy benefit stems from reduced model overfitting. NODEs exhibit a smaller generalization gap compared to conventional models, which we attribute to their constrained expressivity—restricting the modeling of underlying dynamics to a system of differential equations. (3) Moreover, advanced, non-stochastic variants of NODEs can also reduce overfitting, leading to both improved accuracy and a further reduction of membership inference risks.

Our analysis does *not* imply that NODEs are free from membership inference risks. To further mitigate these risks, we study NSDEs, a stochastic extension of NODEs that incorporates an additional diffusion term into system modeling. Most importantly, we *formally show* that this diffusion term functions as a differentially-private (DP) mechanism, thereby establishing NSDEs as DP-learners. Our theoretical analysis shows that the privacy guarantee (ϵ) offered by NSDEs is equivalent to that of DP-SGD when using identical mini-batch training configurations. We demonstrate empirically that NSDEs are more effective at reducing membership risks compared to existing defenses that lack provable privacy guarantees. Unlike DP-SGD, NSDEs achieve this protection with a smaller impact on model utility.

Moreover, we present an effective strategy, *replace-then-finetune*, for using NSDEs as a drop-in privacy-enhancing module. We replace the last few layers of a pre-trained conventional feedforward model with an NSDE block and finetune the adapted model for a few epochs. In evaluation, this strategy reduces the membership inference risks of the original pre-trained model by an order of magnitude, while achieving higher model utility than DP-SGD and requiring only half the training cost (see Appendix for comparisons).

Our work demonstrates that systems learned by neural networks can be effectively *modeled with privacy*. Our findings imply that advanced neural networks incorporating diffusion mechanisms, such as stable diffusion models, may, with careful modeling, serve as inherently private models while preserving its strong performance. As future work, investigating these private systems may offer valuable insights into how DP shapes what learned by neural networks. We also hope our findings inspire the broader adoption of the replace-then-finetune strategy as a practical and effective method for enhancing model privacy.

Acknowledgments

S.H. is partially supported by the Google Faculty Research Award (2023). K.L. acknowledges support from the U.S. National Science Foundation under grant IIS 2338909. A.G. acknowledges support from the U.S. Department of Energy, Office of Advanced Scientific Computing Research under the Scalable, Efficient, and Accelerated Causal Reasoning for Earth and Embedded Systems (SEA-CROGS) project. Sandia National Laboratories is a multimission laboratory managed and operated by National Technology & Engineering Solutions of Sandia, LLC, a wholly owned subsidiary of Honeywell International Inc., for the U.S. Department of Energy's National Nuclear Security Administration under contract DE-NA0003525. This paper describes objective technical results and analysis. Any subjective views or opinions that might be expressed in the paper do not necessarily represent the views of the U.S. Department of Energy or the United States Government. This article has been co-authored by an employee of National Technology & Engineering Solutions of Sandia, LLC under Contract No. DE-NA0003525 with the U.S. Department of Energy (DOE). The employee owns all right, title and interest in and to the article and is solely responsible for its contents. The United States Government retains and the publisher, by accepting the article for publication, acknowledges that the United States Government retains a non-exclusive, paid-up, irrevocable, world-wide license to publish or reproduce the published form of this article or allow others to do so, for United States Government purposes. The DOE will provide public access to these results of federally sponsored research in accordance with the DOE Public Access Plan <https://www.energy.gov/downloads/doe-public-access-plan>.

References

- [1] K. Hornik, M. Stinchcombe, and H. White, "Multilayer feedforward networks are universal approximators," *Neural networks*, vol. 2, no. 5, pp. 359–366, 1989.
- [2] V. Feldman and C. Zhang, "What neural networks memorize and why: Discovering the long tail via influence estimation," *Advances in Neural Information Processing Systems*, vol. 33, pp. 2881–2891, 2020.
- [3] S. Yeom, I. Giacomelli, M. Fredrikson, and S. Jha, "Privacy risk in machine learning: Analyzing the connection to overfitting," in *2018 IEEE 31st Computer Security Foundations Symposium (CSF)*, 2018, pp. 268–282.
- [4] R. Shokri, M. Stronati, C. Song, and V. Shmatikov, "Membership inference attacks against machine learning models," in *2017 IEEE Symposium on Security and Privacy*, 2017, pp. 3–18.
- [5] L. Song and P. Mittal, "Systematic evaluation of privacy risks of machine learning models," in *30th USENIX Security Symposium (USENIX Security 21)*. USENIX Association, Aug. 2021, pp. 2615–2632.
- [6] N. Carlini, S. Chien, M. Nasr, S. Song, A. Terzis, and F. Tramèr, "Membership inference attacks from first principles," in *2022 IEEE Symposium on Security and Privacy (SP)*, 2022, pp. 1897–1914.
- [7] G. Zhang, B. Liu, H. Tian, T. Zhu, M. Ding, and W. Zhou, "How does a deep learning model architecture impact its privacy? a comprehensive study of privacy attacks on CNNs and transformers," in *33rd USENIX Security Symposium (USENIX Security 24)*, 2024, pp. 6795–6812.
- [8] R. T. Q. Chen, Y. Rubanova, J. Bettencourt, and D. K. Duvenaud, "Neural Ordinary Differential Equations," in *Advances in Neural Information Processing Systems*, vol. 31, 2018.
- [9] P. Kidger, J. Morrill, J. Foster, and T. Lyons, "Neural Controlled Differential Equations for Irregular Time Series," *Advances in Neural Information Processing Systems*, 2020.
- [10] J. Jeon, J. KIM, H. Song, S. Cho, and N. Park, "GT-GAN: General purpose time series synthesis with generative adversarial networks," in *Advances in Neural Information Processing Systems*, 2022.
- [11] F. Wu, W. Cho, D. Korotky, S. Hong, D. Rim, N. Park, and K. Lee, "Identifying contemporaneous and lagged dependence structures by promoting sparsity in continuous-time neural networks," in *Proceedings of the 33rd ACM International Conference on Information and Knowledge Management*, 2024, pp. 2534–2543.
- [12] S. Greydanus, M. Dzamba, and J. Yosinski, "Hamiltonian neural networks," *Advances in neural information processing systems*, vol. 32, 2019.
- [13] Y. Verma, M. Heinonen, and V. Garg, "ClimODE: Climate and weather forecasting with physics-informed neural ODEs," in *The Twelfth International Conference on Learning Representations*, 2024.
- [14] K. Lee, N. Trask, and P. Stinis, "Machine learning structure preserving brackets for forecasting irreversible processes," *Advances in Neural Information Processing Systems*, vol. 34, pp. 5696–5707, 2021.
- [15] A. Gruber, K. Lee, and N. Trask, "Reversible and irreversible bracket-based dynamics for deep graph neural networks," *Advances in Neural Information Processing Systems*, vol. 36, 2024.
- [16] E. Dupont, A. Doucet, and Y. W. Teh, "Augmented neural odes," *Advances in Neural Information Processing Systems*, vol. 32, 2019.
- [17] C. Yildiz, M. Heinonen, and H. Lahdesmaki, "Ode2vae: Deep generative second order odes with bayesian neural networks," *Advances in Neural Information Processing Systems*, vol. 32, 2019.
- [18] H. Xia, V. Suliafu, H. Ji, T. M. Nguyen, A. Bertozzi, S. Osher, and B. Wang, "Heavy ball neural ordinary differential equations," in *Advances in Neural Information Processing Systems*, 2021.
- [19] S. Cho, S. Hong, K. Lee, and N. Park, "AdamNODEs: When neural ODE meets adaptive moment estimation," 2022.
- [20] K. He, X. Zhang, S. Ren, and J. Sun, "Deep residual learning for image recognition," in *Proceedings of the IEEE conference on computer vision and pattern recognition*, 2016, pp. 770–778.
- [21] A. Norcliffe, C. Bodnar, B. Day, N. Simidjievski, and P. Liò, "On second order behaviour in augmented neural networks," *Advances in Neural Information Processing Systems*, vol. 33, pp. 5911–5921, 2020.
- [22] X. Liu, T. Xiao, S. Si, Q. Cao, S. Kumar, and C.-J. Hsieh, "Neural SDE: Stabilizing neural ode networks with stochastic noise," *arXiv preprint arXiv:1906.02355*, 2019.
- [23] M. Abadi, A. Chu, I. Goodfellow, H. B. McMahan, I. Mironov, K. Talwar, and L. Zhang, "Deep learning with differential privacy," in *Proceedings of the 2016 ACM SIGSAC Conference on Computer and Communications Security*, ser. CCS '16, 2016, p. 308–318.
- [24] Y. Kaya, S. Hong, and T. Dumitras, "On the effectiveness of regularization against membership inference attacks," *CoRR*, vol. abs/2006.05336, 2020.
- [25] S. H. Strogatz, *Nonlinear Dynamics and Chaos: With Applications to Physics, Biology, Chemistry, and Engineering*. CRC press, 2018.
- [26] Y. Rubanova, R. T. Chen, and D. K. Duvenaud, "Latent ordinary differential equations for irregularly-sampled time series," *Advances in neural information processing systems*, vol. 32, 2019.
- [27] L. S. Pontryagin, *Mathematical Theory of Optimal Processes*. Routledge, 2018.

- [28] N. Nguyen, T. M. Nguyen, V. T. K. Huyen, S. Osher, and T. Vo, "Improving neural ordinary differential equations with Nesterov's accelerated gradient method," in *Advances in Neural Information Processing Systems*, 2022.
- [29] X. Li, T.-K. L. Wong, R. T. Chen, and D. Duvenaud, "Scalable gradients for stochastic differential equations," in *International Conference on Artificial Intelligence and Statistics*. PMLR, 2020, pp. 3870–3882.
- [30] P. Kidger, J. Foster, X. Li, and T. J. Lyons, "Neural SDEs as infinite-dimensional GANs," in *International conference on machine learning*. PMLR, 2021, pp. 5453–5463.
- [31] E. Platen and N. Bruti-Liberati, *Numerical solution of stochastic differential equations with jumps in finance*. Springer Science & Business Media, 2010, vol. 64.
- [32] X. Liu, T. Xiao, S. Si, Q. Cao, S. Kumar, and C.-J. Hsieh, "How does noise help robustness? explanation and exploration under the neural sde framework," in *Proceedings of the IEEE/CVF Conference on Computer Vision and Pattern Recognition (CVPR)*, June 2020.
- [33] C. Dwork, "Differential privacy," in *International colloquium on automata, languages, and programming*. Springer, 2006, pp. 1–12.
- [34] L. Watson, C. Guo, G. Cormode, and A. Sablayrolles, "On the importance of difficulty calibration in membership inference attacks," in *International Conference on Learning Representations*, 2022.
- [35] S. Zarifzadeh, P. Liu, and R. Shokri, "Low-cost high-power membership inference attacks," in *Proceedings of the 41st International Conference on Machine Learning*, 2024, pp. 58 244–58 282.
- [36] J. Jia, A. Salem, M. Backes, Y. Zhang, and N. Z. Gong, "MemGuard: Defending against black-box membership inference attacks via adversarial examples," in *Proceedings of the 2019 ACM SIGSAC Conference on Computer and Communications Security*, ser. CCS '19, 2019, p. 259–274.
- [37] J. Li, N. Li, and B. Ribeiro, "Membership inference attacks and defenses in classification models," in *Proceedings of the Eleventh ACM Conference on Data and Application Security and Privacy*, ser. CODASPY '21, 2021, p. 5–16.
- [38] Y. Song, J. Sohl-Dickstein, D. P. Kingma, A. Kumar, S. Ermon, and B. Poole, "Score-based generative modeling through stochastic differential equations," in *International Conference on Learning Representations*, 2021.
- [39] M. Nasr, R. Shokri, and A. Houmansadr, "Comprehensive privacy analysis of deep learning: Passive and active white-box inference attacks against centralized and federated learning," in *2019 IEEE Symposium on Security and Privacy*. IEEE, 2019, pp. 739–753.
- [40] H. Xiao, K. Rasul, and R. Vollgraf, "Fashion-MNIST: A novel image dataset for benchmarking machine learning algorithms," *arXiv preprint arXiv:1708.07747*, 2017.
- [41] A. Krizhevsky, "Learning multiple layers of features from tiny images," Tech. Rep., 2009.
- [42] J. Deng, W. Dong, R. Socher, L.-J. Li, K. Li, and L. Fei-Fei, "ImageNet: A large-scale hierarchical image database," in *IEEE Conference on Computer Vision and Pattern Recognition (CVPR)*, 2009, pp. 248–255.
- [43] V. Oganessian, A. Volokhova, and D. Vetrov, "Stochasticity in neural ODEs: An empirical study," *arXiv preprint arXiv:2002.09779*, 2020.
- [44] C. Dwork and A. Roth, "The algorithmic foundations of differential privacy," *Foundations and Trends in Theoretical Computer Science*, vol. 9, no. 3–4, pp. 211–407, 2014.
- [45] R. Wang and I. Manchester, "Direct parameterization of Lipschitz-bounded deep networks," in *International Conference on Machine Learning*. PMLR, 2023, pp. 36 093–36 110.
- [46] J. Dong, A. Roth, and W. J. Su, "Gaussian differential privacy," *Journal of the Royal Statistical Society: Series B (Statistical Methodology)*, vol. 84, no. 1, pp. 3–37, 2022.
- [47] N. Ponomareva, S. Vassilvitskii, Z. Xu, B. McMahan, A. Kurakin, and C. Zhang, "How to DP-fy ML: A practical tutorial to machine learning with differential privacy," in *Proceedings of the 29th ACM SIGKDD Conference on Knowledge Discovery and Data Mining*, ser. KDD '23, 2023, p. 5823–5824.
- [48] C. A. Choquette-Choo, F. Tramer, N. Carlini, and N. Papernot, "Label-only membership inference attacks," in *International conference on machine learning*. PMLR, 2021, pp. 1964–1974.
- [49] B. Jayaraman and D. Evans, "Evaluating differentially private machine learning in practice," in *28th USENIX Security Symposium (USENIX Security 19)*, Aug. 2019, pp. 1895–1912.
- [50] F. Tramer and D. Boneh, "Differentially private learning needs better features (or much more data)," in *International Conference on Learning Representations*, 2021.
- [51] M. Fredrikson, E. Lantz, S. Jha, S. Lin, D. Page, and T. Ristenpart, "Privacy in pharmacogenetics: An end-to-end case study of personalized warfarin dosing," in *USENIX Security Symposium*, 2014.
- [52] M. Fredrikson, S. Jha, and T. Ristenpart, "Model inversion attacks that exploit confidence information and basic countermeasures," in *Proceedings of the 22nd ACM SIGSAC Conference on Computer and Communications Security*, ser. CCS '15, 2015, p. 1322–1333.
- [53] X. Wu, M. Fredrikson, S. Jha, and J. F. Naughton, "A methodology for formalizing model-inversion attacks," in *2016 IEEE 29th Computer Security Foundations Symposium (CSF)*, 2016, pp. 355–370.
- [54] S. Mehnaz, S. V. Dibbo, E. Kabir, N. Li, and E. Bertino, "Are your sensitive attributes private? novel model inversion attribute inference attacks on classification models," in *31st USENIX Security Symposium (USENIX Security 22)*, Aug. 2022, pp. 4579–4596.
- [55] E. Zheleva and L. Getoor, "To join or not to join: The illusion of privacy in social networks with mixed public and private user profiles," in *Proceedings of the 18th International Conference on World Wide Web*, ser. WWW '09, 2009, p. 531–540.
- [56] A. Chaabane, G. Acs, M. A. Kaafar *et al.*, "You are what you like! information leakage through users' interests," in *Proceedings of the 19th annual network & distributed system security symposium (NDSS)*. Citeseer, 2012.
- [57] N. Z. Gong, A. Talwalkar, L. Mackey, L. Huang, E. C. R. Shin, E. Stefanov, E. R. Shi, and D. Song, "Joint link prediction and attribute inference using a social-attribute network," *ACM Trans. Intell. Syst. Technol.*, vol. 5, no. 2, Apr. 2014.
- [58] N. Z. Gong and B. Liu, "You are who you know and how you behave: Attribute inference attacks via users' social friends and behaviors," in *25th USENIX Security Symposium (USENIX Security 16)*, Aug. 2016, pp. 979–995.
- [59] J. Jia, B. Wang, L. Zhang, and N. Z. Gong, "AttriInfer: Inferring user attributes in online social networks using Markov random fields," in *Proceedings of the 26th International Conference on World Wide Web*, ser. WWW '17, 2017, p. 1561–1569.
- [60] N. Z. Gong and B. Liu, "Attribute inference attacks in online social networks," *ACM Trans. Priv. Secur.*, vol. 21, no. 1, Jan. 2018.
- [61] U. Weinsberg, S. Bhagat, S. Ioannidis, and N. Taft, "BlurMe: Inferring and obfuscating user gender based on ratings," in *Proceedings of the Sixth ACM Conference on Recommender Systems*, ser. RecSys '12, 2012, p. 195–202.
- [62] L. Wu, Y. Yang, K. Zhang, R. Hong, Y. Fu, and M. Wang, "Joint item recommendation and attribute inference: An adaptive graph convolutional network approach," in *Proceedings of the 43rd International ACM SIGIR Conference on Research and Development in Information Retrieval*, ser. SIGIR '20, New York, NY, USA, 2020, p. 679–688.
- [63] N. Carlini, C. Liu, Ú. Erlingsson, J. Kos, and D. Song, "The secret sharer: Evaluating and testing unintended memorization in neural networks," in *28th USENIX Security Symposium (USENIX Security 19)*, Aug. 2019, pp. 267–284.

- [64] N. Carlini, F. Tramèr, E. Wallace, M. Jagielski, A. Herbert-Voss, K. Lee, A. Roberts, T. Brown, D. Song, Ú. Erlingsson, A. Oprea, and C. Raffel, “Extracting training data from large language models,” in *30th USENIX Security Symposium (USENIX Security 21)*, Aug. 2021, pp. 2633–2650.
- [65] N. Carlini, J. Hayes, M. Nasr, M. Jagielski, V. Schwag, F. Tramèr, B. Balle, D. Ippolito, and E. Wallace, “Extracting training data from diffusion models,” in *32nd USENIX Security Symposium (USENIX Security 23)*, Aug. 2023, pp. 5253–5270.
- [66] I. Goodfellow, J. Shlens, and C. Szegedy, “Explaining and harnessing adversarial examples,” in *International Conference on Learning Representations*, 2015.
- [67] Y. Hanshu, D. Jiawei, T. Vincent, and F. Jiashi, “On robustness of neural ordinary differential equations,” in *International Conference on Learning Representations*, 2020.
- [68] Q. Kang, Y. Song, Q. Ding, and W. P. Tay, “Stable neural ODE with Lyapunov-stable equilibrium points for defending against adversarial attacks,” *Advances in Neural Information Processing Systems*, vol. 34, pp. 14 925–14 937, 2021.
- [69] X. Li, Z. Xin, and W. Liu, “Defending against adversarial attacks via neural dynamic system,” *Advances in Neural Information Processing Systems*, vol. 35, pp. 6372–6383, 2022.
- [70] M. Zeqiri, M. N. Mueller, M. Fischer, and M. Vechev, “Efficient certified training and robustness verification of neural ODEs,” in *The Eleventh International Conference on Learning Representations*, 2023.
- [71] Y. Huang, Y. Yu, H. Zhang, Y. Ma, and Y. Yao, “Adversarial robustness of stabilized neural ODE might be from obfuscated gradients,” in *Mathematical and Scientific Machine Learning*. PMLR, 2022, pp. 497–515.
- [72] S. Anumasa and P. Sriyith, “Improving robustness and uncertainty modelling in neural ordinary differential equations,” in *Proceedings of the IEEE/CVF Winter Conference on Applications of Computer Vision*, 2021, pp. 4053–4061.
- [73] C. Finlay, J.-H. Jacobsen, L. Nurbekyan, and A. Oberman, “How to train your neural ODE: The world of Jacobian and kinetic regularization,” in *International conference on machine learning*. PMLR, 2020, pp. 3154–3164.
- [74] J. Kelly, J. Bettencourt, M. J. Johnson, and D. K. Duvenaud, “Learning differential equations that are easy to solve,” *Advances in Neural Information Processing Systems*, vol. 33, pp. 4370–4380, 2020.
- [75] A. Ghosh, H. Behl, E. Dupont, P. Torr, and V. Nambodiri, “Steer: Simple temporal regularization for neural ODE,” *Advances in Neural Information Processing Systems*, vol. 33, pp. 14 831–14 843, 2020.
- [76] S. Jha, R. Ewetz, A. Velasquez, and S. Jha, “On smoother attributions using neural stochastic differential equations,” in *30th International Joint Conference on Artificial Intelligence (IJCAI)*, 2021, 2021.
- [77] L. Kong, J. Sun, and C. Zhang, “SDE-Net: Equipping deep neural networks with uncertainty estimates,” in *International Conference on Machine Learning*. PMLR, 2020, pp. 5405–5415.

Appendix

A. Model Architectures

We adopt architectures examined in prior work [43].

ResNet-14 is defined as

$$[\text{Conv2d} \rightarrow \text{BN} \rightarrow [\text{ResBlock} \times 3 \rightarrow \text{BN} \rightarrow \text{Conv2d}] \times 2 \rightarrow \text{ResBlock} \times 3 \rightarrow \text{AdaptiveAvgPool2d} \rightarrow \text{Linear}],$$

where ResBlock is composed as $[\text{BN} \rightarrow \text{Conv2d} \rightarrow \text{BN} \rightarrow \text{Conv2d}]$.

ODENet-16-32-64 is defined same as ResNet-14 except that ResBlock is replaced with ODEBlock, which is defined as $[\text{ConcatConv2d} \rightarrow \text{ConcatConv2d}]$, where ConcatConv2d augments x by concatenating an additional feature channel derived from t .

Both models begin with Conv2d that processes a 3-channel input image to produce 32 feature maps using a 3×3 filter with a stride of 2 and padding of 1. Following the initial convolutional layer, the features pass through a group of either three ResBlocks or a single ODEBlock, depending on the configuration. Subsequently, the network transitions through a Downsampling layer, which effectively reduces the spatial dimensions while adjust the channel depth, preparing the features for subsequent layers. After the third group of three ResBlocks or an ODEBlock, the network utilizes an adaptive average pooling layer to condenses the feature maps into a single dimensional vector per feature map. This vector is then flattened and passed through a linear layer which acts as the classifier of the network, outputting the final predictions across the categories.

B. Differential Privacy of Gaussian Mechanism

The following result is proved in [44]. Since it is crucial to the results in the body, a slightly different proof is provided here for completeness.

Proposition 1 (Theorem A.1 in [44]). Let $\varepsilon \in (0, 1)$. The Gaussian mechanism, $M(\mathbf{q}) = \mathbf{f}(\mathbf{q}) + \mathcal{N}(0, \sigma^2 \mathbf{I})$ with variance parameter $\sigma \geq \sqrt{2 \ln(1.25/\delta)} (S_{\mathbf{f}}/\varepsilon)$ is (ε, δ) -differentially private.

Proof. Consider two adjacent datasets \mathbf{q}, \mathbf{q}' , i.e., $|\mathbf{q} - \mathbf{q}'| < 1$. Without loss of generality, write $\mathbf{f}(\mathbf{q}) = \mathbf{f}(\mathbf{q}') + \mathbf{v}$ for some $\mathbf{v} \in \mathbb{R}^n$. Drawing $\mathbf{X} \sim \mathcal{N}(\mathbf{0}, \sigma^2 \mathbf{I})$, the proof is based on analyzing the privacy loss random variable,

$$\begin{aligned} \ln \left(\frac{\Pr[M(\mathbf{q}) = \mathbf{f}(\mathbf{q}) + \mathbf{X}]}{\Pr[M(\mathbf{q}') = \mathbf{f}(\mathbf{q}') + \mathbf{X}]} \right) &= \ln \left(\frac{\exp\left(\frac{-1}{2\sigma^2} |\mathbf{X}|^2\right)}{\exp\left(\frac{-1}{2\sigma^2} |\mathbf{X} + \mathbf{v}|^2\right)} \right) \\ &= \frac{1}{2\sigma^2} \left(|\mathbf{X} + \mathbf{v}|^2 - |\mathbf{X}|^2 \right) = \frac{\langle \mathbf{v}, \mathbf{X} \rangle}{\sigma^2} + \frac{|\mathbf{v}|^2}{2\sigma^2}, \end{aligned}$$

which is normally distributed with mean $|\mathbf{v}|^2 / (2\sigma^2)$ and variance $|\mathbf{v}|^2 / \sigma^2$. Choosing $\mathbf{Z} \sim \mathcal{N}(\mathbf{0}, \mathbf{I})$, the privacy loss random variable is bounded by ε when

$$\left| \frac{|\mathbf{v}|}{\sigma} \mathbf{Z} + \frac{|\mathbf{v}|^2}{2\sigma^2} \right| \leq \frac{|\mathbf{v}|}{\sigma} \left(|\mathbf{Z}| + \frac{|\mathbf{v}|}{2\sigma} \right) \leq \varepsilon.$$

In view of this, it suffices to bound the tail probability

$$\Pr \left[|\mathbf{Z}| > \frac{\varepsilon\sigma}{|\mathbf{v}|} - \frac{|\mathbf{v}|}{2\sigma} \right] = 2 \Pr \left[\mathbf{Z} > \frac{\varepsilon\sigma}{|\mathbf{v}|} - \frac{|\mathbf{v}|}{2\sigma} \right] < \delta.$$

Choosing the standard deviation $\sigma = t|\mathbf{v}|/\varepsilon$ for some $t > 0$ to be determined, Mill’s inequality guarantees that it is enough to require

$$\Pr \left[\mathbf{Z} > t - \frac{\varepsilon}{2t} \right] \leq \frac{1}{\sqrt{2\pi}(t - \varepsilon/2t)} \exp\left(-\frac{1}{2}(t - \varepsilon/2t)^2\right) < \delta/2$$

TABLE 5. MEMBERSHIP INFERENCE RISKS OF ODENET-64 MODELS AND SDENET $\sigma=0$ MODELS. WE EVALUATE ODENET-64 MODELS AND SDENET $\sigma=0$ MODELS AGAINST SIX EXISTING ATTACKS ON CIFAR-10 AND CIFAR-100.

Model	Method	Acc. (C-10)		Acc. (C-100)		TPR @ 0.1% FPR		TPR @ 1% FPR		AUC		Inference acc.	
		Train	Test	Train	Test	C-10	C-100	C-10	C-100	C-10	C-100	C-10	C-100
ODENet-64	Yeom et al. [3]					0.00%	0.03%	0.28%	1.17%	0.536	0.659	53.57%	66.09%
	Shokri et al. [4]					0.08%	0.09%	0.75%	0.85%	0.473	0.480	50.03%	50.01%
	Song and Mittal [38]	94.14%	84.36%	70.93%	51.85%	0.01%	0.13%	0.53%	1.58%	0.511	0.497	51.17%	51.63%
	Watson et al. [34]					0.00%	0.03%	0.28%	1.17%	0.536	0.659	53.57%	66.09%
	Carlini et al. [6]					0.86%	1.72%	4.17%	7.70%	0.639	0.741	59.57%	69.49%
	Zarifzadeh et al. [35]					2.72%	2.91%	8.40%	11.47%	0.617	0.757	59.96%	70.65%
SDENet $\sigma=0$	Yeom et al. [3]					0.00%	0.09%	0.39%	1.12%	0.538	0.625	54.00%	60.52%
	Shokri et al. [4]					0.07%	0.05%	0.68%	0.63%	0.468	0.449	50.02%	50.00%
	Song and Mittal [38]	89.09%	83.93%	68.01%	52.49%	0.00%	0.14%	0.50%	1.40%	0.516	0.496	51.65%	51.13%
	Watson et al. [34]					0.00%	0.09%	0.44%	1.12%	0.538	0.625	54.00%	60.52%
	Carlini et al. [6]					0.35%	1.03%	2.02%	5.36%	0.559	0.676	54.09%	62.26%
	Zarifzadeh et al. [35]					0.91%	2.04%	4.01%	8.04%	0.579	0.701	55.76%	63.58%

or, said differently, it is enough to choose t such that

$$\ln\left(t - \frac{\varepsilon}{2t}\right) + \frac{1}{2}\left(t - \frac{\varepsilon}{2t}\right)^2 > \ln\left(\frac{1}{\delta}\sqrt{\frac{2}{\pi}}\right).$$

Note that, by enforcing $t \geq 1$ and $0 < \varepsilon < 1$, the first term on the left-hand side is nonnegative when $t - \frac{\varepsilon}{2t} \geq t - \frac{1}{2} \geq 1$. Therefore, it suffices to choose $t \geq 3/2$ to ensure positivity. On the other hand, the second term is increasing in t when $t > \sqrt{\varepsilon/2}$ and decreasing in ε when $\varepsilon < 2t^2$, so it follows that we may ensure

$$\left(t - \frac{\varepsilon}{2t}\right)^2 = t^2 - \varepsilon + \left(\frac{\varepsilon}{2t}\right)^2 \geq t^2 - 1 + 1 \cdot 3^{-2} = t^2 - \frac{8}{9} > 2 \ln\left(\frac{1}{\delta}\sqrt{\frac{2}{\pi}}\right).$$

This implies that

$$t^2 > 2 \ln\left(\frac{1}{\delta}\sqrt{\frac{2}{\pi}}\right) + \ln\left(e^{8/9}\right) = 2 \ln\left(\frac{1}{\delta}\right) + \ln\left(e^{8/9}\frac{2}{\pi}\right)$$

and since $(2/\pi)e^{8/9} < 1.25^2$, this condition is satisfied when $t^2 > 2 \ln\left(\frac{1.25}{\delta}\right)$. This shows that the privacy loss random variable is bounded above by ε with probability $1 - \delta$ on \mathbf{q}, \mathbf{q}' whenever $\sigma \geq \sqrt{2 \ln(1.25/\delta)}(|v|/\varepsilon)$. To remove the dependence on \mathbf{q}, \mathbf{q}' , it suffices to choose $\sigma \geq \sqrt{2 \ln(1.25/\delta)}(S_{\mathbf{f}}/\varepsilon)$. \square

C. Additional Evaluation Results

Membership risks of NODEs, based on ODENet-64 architecture. Table 5 summarizes our additional results on NODE (ODENet-64) models and NSDEs with $\sigma = 0$, respectively. It is notable that ODENet-64 demonstrates comparable results to ODENet-16_32_64 but with a decrease in test accuracy of 1.64% and 2.41% on CIFAR-10 and CIFAR-100, respectively. It is 2.5-6 \times less susceptible to LiRA attacks compared to ResNet-14. On CIFAR-100, ODENet exhibits superior defense capabilities against LiRA attacks than ODENet-16_32_64, demonstrating a lower TPR@0.1%FPR of 1.72%, thereby demonstrating enhanced security against membership inference attacks compared to ResNet-14. For NSDEs with $\sigma = 0$, despite being the non-privacy variant, it exhibits robust defense capabilities. NSDEs with $\sigma = 0$ maintains competitive test

accuracy and generalization gaps on both CIFAR datasets. Notably, NSDEs $\sigma=0$ showcases its strengths in defending against membership inference attacks, with TPR@0.1%FPR of 0.35% and 1.03% for CIFAR-10 and CIFAR-100, respectively, demonstrating a stronger defense compared to ResNet-14 and NODE models. This superior performance in TPR@0.1%FPR, coupled with robust accuracy metrics, underscores NSDE’s ability to enhance security against advanced threats.

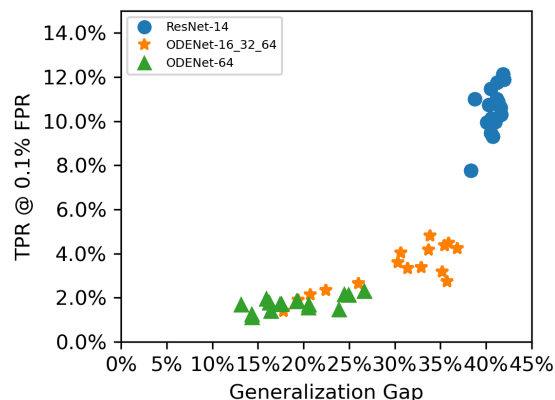


Figure 8. Membership risks and overfitting in CIFAR-100.

Impact of generalization gap in attack success (CIFAR-100). Figure 8 illustrates the relationship between membership risks measured by LiRA and the generalization gap for models trained on CIFAR-100. For ResNet-14, the TPR at 0.1% FPR ranges from 8%–14%, even as the generalization gap remains consistently around 40%. This suggests that overfitting contributes to membership inference risks. In contrast, NODEs (ODENet-16_32_64 and ODENet-64) show slightly lower generalization gaps, typically ranging from 19.08%–30%. Their TPR at 0.1% FPR values are also lower, fluctuating between 0.5%–5.5%. This suggests that NODEs are less prone to overfitting, thereby reducing their risks to membership inference attacks.

Membership risks of replace-then-finetune strategy. We

analyze the computational resources required for training ResNet, NODEs, NSDEs and NSDEs with replace-then-finetune models. As shown in Table 6, training NSDE-based models from scratch is computationally expensive. Table 7 demonstrates the results with membership inference risks of replace-then-finetune strategy. We evaluate NSDEs with replace-then-finetune models against six existing attacks on four datasets. Although only replacing the final blocks of a ResNet with SDENet, the replace-then-finetune models narrows the generation gap while achieving lower TPR at both 0.1% and 1% FPR across four dataset, indicating improved robustness compared to the ResNet models.

Figure and tables for additional results. Here, we present full experimental results to support the findings reported in the main body of the manuscript: Tables 8–11, where each table covers specific aspects. Table 8 demonstrates the results with varying number of blocks of models in Figure 2 and 6. Table 9 and 10 provide supporting data for Figure 2, illustrating the results of the impact of solvers and variants for NODEs. The detailed evaluation results of defenses, which provide an in-depth analysis corresponding to Figure 3, are presented in Table 11.

TABLE 6. COMPUTATIONAL RESOURCES REQUIRED FOR TRAINING ON CIFAR-10 AND CIFAR-100.

Model	Time per epoch	Memory usage
ResNet-14	10s	941MB
NODE (ODENet-16-32-64)_block1	23s	1305MB
NSDE (SDENet $k=2$)_block1	30s	5051MB
NSDE (replace-then-finetune)	15s	1575MB

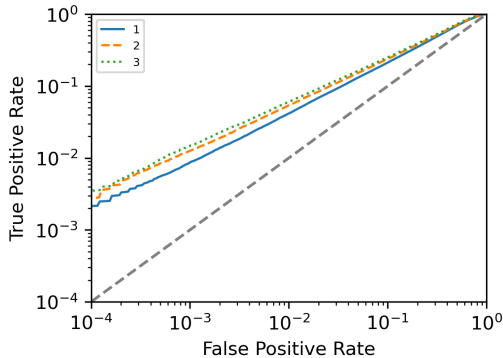


Figure 9. **Membership inference risks of ODENet-64 models.** We evaluate ODENet-64 models with varying numbers of NODE blocks against the attack of LiRA in CIFAR-10.

TABLE 7. MEMBERSHIP RISKS OF REPLACE-AND-FINETUNE STRATEGY RESNET+SDENET.

Method	TPR @ 0.1% FPR				TPR @ 1% FPR				AUC				Inference acc.			
	F-M	C-10	C-100	T-I	F-M	C-10	C-100	T-I	F-M	C-10	C-100	T-I	F-M	C-10	C-100	T-I
Yeom et al. [3]	0.01%	0.00%	0.07%	0.09%	0.06%	0.14%	1.10%	1.12%	0.558	0.555	0.646	0.638	55.72%	55.81%	64.41%	61.22%
Shokri et al. [4]	0.06%	0.05%	0.05%	0.12%	0.65%	0.52%	0.56%	1.04%	0.477	0.450	0.433	0.502	50.01%	50.00%	50.00%	50.20%
Song and Mittal [38]	0.00%	0.01%	0.13%	0.13%	0.24%	0.24%	1.48%	1.19%	0.468	0.530	0.496	0.500	51.05%	53.29%	51.15%	50.36%
Watson et al. [34]	0.00%	0.00%	0.07%	0.11%	0.10%	0.15%	1.10%	1.17%	0.550	0.555	0.646	0.537	53.81%	55.81%	64.41%	52.83%
Carlini et al. [6]	1.39%	0.45%	1.65%	0.21%	4.48%	2.84%	7.51%	1.57%	0.576	0.600	0.726	0.535	53.27%	56.78%	67.37%	52.42%
Zarifzadeh et al. [35]	0.73%	1.41%	2.91%	0.26%	4.74%	5.68%	10.88%	1.89%	0.544	0.607	0.743	0.561	54.80%	57.97%	68.67%	54.54%

TABLE 8. COMPARING MEMBERSHIP RISKS OF NODES AND NSDES. WE VARY THE NUMBER OF BLOCKS IN {1, 2, 3} AND USE LiRA.

Model	# of Blocks	Acc. (C-10)		Acc. (C-100)		TPR @ 0.1% FPR		TPR @ 1% FPR		AUC		Inference acc.	
		Train	Test	Train	Test	C-10	C-100	C-10	C-100	C-10	C-100	C-10	C-100
ODENet-16_32_64	1	94.30%	84.41%	82.05%	52.16%	1.01%	3.30%	4.22%	12.11%	0.616	0.782	57.65%	72.88%
	2	96.39%	85.26%	93.40%	52.8%	1.57%	7.01%	5.95%	20.86%	0.638	0.848	58.99%	75.77%
	3	96.82%	85.25%	94.71%	53.07%	1.66%	7.78%	6.17%	22.38%	0.641	0.852	58.86%	76.32%
ODENet-64	1	94.14%	84.36%	70.93%	51.85%	0.86%	1.72%	4.17%	7.70%	0.639	0.741	59.57%	69.49%
	2	97.07%	85.20%	80.74%	53.39%	1.25%	2.41%	5.43%	10.59%	0.656	0.788	60.78%	64.33%
	3	97.74%	85.82%	87.26%	53.78%	1.49%	3.29%	6.05%	13.71%	0.669	0.815	60.89%	69.85%
SDENet-16_32_64	1	81.89%	81.91%	56.54%	50.64%	0.14%	0.43%	1.24%	3.00%	0.525	0.612	51.89%	57.64%
	2	82.41%	82.42%	57.20%	51.12%	0.14%	0.45%	1.25%	2.99%	0.528	0.619	52.23%	58.57%
	3	74.44%	74.96%	55.73%	48.27%	0.08%	0.32%	0.90%	2.58%	0.511	0.604	50.00%	57.43%

TABLE 9. MEMBERSHIP RISKS OF NODES TRAINED WITH DIFFERENT SOLVERS. WE COMPARE THE LiRA SUCCESS ON THEM.

Model	Solver	Acc. (C-10)		Acc. (C-100)		TPR @ 0.1% FPR		TPR @ 1% FPR		AUC		Inference acc.	
		Train	Test	Train	Test	C-10	C-100	C-10	C-100	C-10	C-100	C-10	C-100
ODENet-16_32_64	Euler	94.30%	84.41%	82.05%	52.16%	1.01%	3.30%	4.22%	12.11%	0.616	0.782	57.65%	72.88%
	Rk4	94.28%	84.39%	83.32%	52.19%	0.89%	3.70%	4.02%	13.07%	0.617	0.792	57.78%	73.05%
	Dopri5	94.41%	84.61%	80.20%	52.20%	0.68%	3.02%	3.40%	11.20%	0.609	0.777	57.43%	64.34%

TABLE 10. MEMBERSHIP RISKS OF NODE VARIANTS. WE COMPARE THE LiRA SUCCESS ON THESE MODELS IN CIFAR-10.

Model	Acc. (Train)	Acc. (Test)	Train-Test Acc. Gap	TPR @ 0.1% FPR	TPR @ 1% FPR	AUC	Inference acc.
SONODE	92.35%	86.52%	5.9%	0.44%	2.62%	0.585	55.81%
ANODE(+64)	89.09%	85.10%	4.0%	0.35%	2.15%	0.572	55.07%
ANODE(+16)	87.60%	84.62%	3.0%	0.24%	1.76%	0.558	54.10%
HBNODE	84.91%	82.11%	2.8%	0.24%	1.74%	0.545	53.10%
ODENet-64 (Baseline)	94.14%	84.36%	9.7%	0.86%	4.17%	0.639	59.57%

TABLE 11. EFFECTIVENESS OF DEFENSES IN CIFAR-10. WE USE LiRA. ALL DEFENSES, EXCEPT FOR SDENETS, ARE APPLIED TO RESNET-14.

Model	Acc. (Train)	Acc. (Test)	Train-Test Acc. Gap	TPR @ 0.1% FPR	TPR @ 1% FPR	AUC	Inference acc.
Memguard	98.14%	85.97%	12.17%	0.00%	0.00%	0.580	54.48%
MMD+mix-up	95.10%	87.39%	7.71%	2.03%	7.09%	0.628	57.95%
L2-Regularization	98.84%	86.60%	12.24%	2.36%	7.81%	0.675	61.54%
L1-Regularization	97.39%	86.48%	10.91%	1.06%	4.77%	0.641	59.47%
DP-SGD, $\epsilon=8$	73.49%	74.44%	-0.95%	0.12%	1.18%	0.516	51.28%
ResNet-14	98.14%	85.97%	12.17%	3.96%	10.57%	0.679	61.15%
SDENet $\sigma=0$	89.09%	83.93%	5.16%	0.35%	2.02%	0.559	54.09%
SDENet $\sigma=2$	81.89%	81.91%	-0.02%	0.14%	1.24%	0.525	51.89%

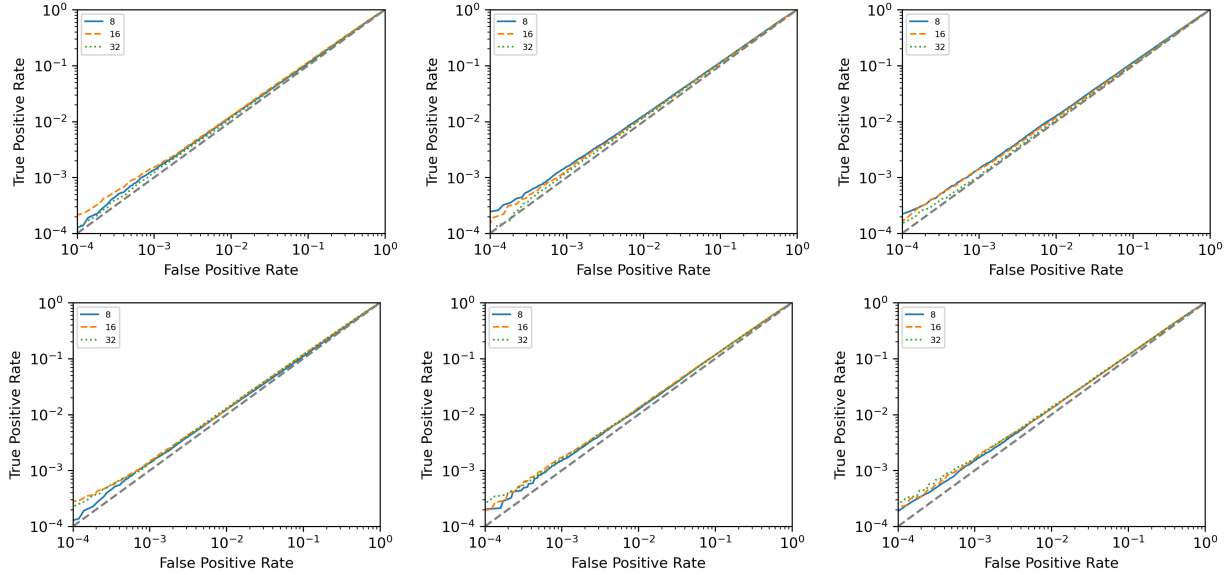


Figure 10. Membership risks of NSDEs train with different step-size ($1/s$). (Top row, left to right) We illustrate the impact of step-size ($1/s$) with the level of stochasticity $k=0.5$, and varying the integration Time $T=0.5, 0.25, 0.125$, respectively. (Bottom row, left to right) We illustrate the impact of step-size ($1/s$) with the level of noise intensity $\sigma=2$, and varying the integration Time $T=0.5, 0.25, 0.125$, respectively.

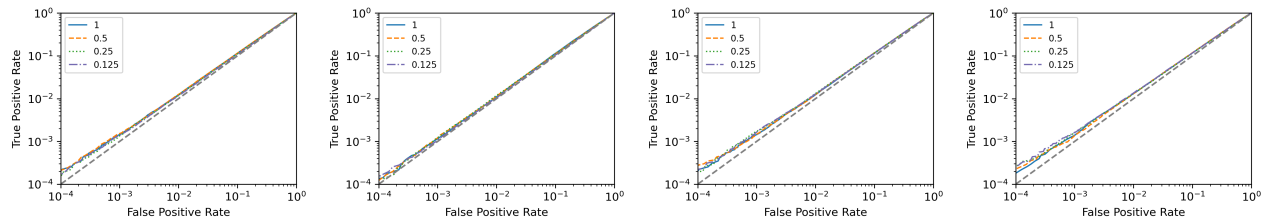


Figure 11. Membership risks of NSDEs train with different time interval (T). We illustrate the impact of time (T) with the level of stochasticity $k=0.5$ (left two) and noise intensity $\sigma=2$ (right two), and varying $s=16, 32$, respectively.

TABLE 12. FULL EVALUATION RESULTS OF DIFFERENT NSDE CONFIGURATIONS.

Impact	Step_size	Time	Stochasticity	Noise	Train Acc.	Test Acc.	TPR @ 0.1% FPR	TPR @ 1% FPR	AUC	Inference acc.
Step_size	8	1	0.5	1.4	83.27%	82.38%	0.15%	1.37%	0.527	52.04%
	16	1	0.5	2	81.89%	81.91%	0.14%	1.24%	0.525	51.89%
	32	1	0.5	2.8	46.65%	35.86%	0.14%	1.29%	0.523	52.10%
Step_size	8	0.5	0.5	2	83.09%	82.52%	0.14%	1.27%	0.527	51.60%
	16	0.5	0.5	2.8	81.61%	82.00%	0.15%	1.26%	0.527	51.99%
	32	0.5	0.5	4	79.26%	80.92%	0.14%	1.15%	0.519	51.37%
Step_size	8	0.25	0.5	2.8	82.40%	82.05%	0.16%	1.27%	0.525	51.88%
	16	0.25	0.5	4	80.89%	81.21%	0.13%	1.20%	0.521	51.59%
	32	0.25	0.5	5.7	77.90%	80.12%	0.12%	1.19%	0.514	50.84%
Step_size	8	0.125	0.5	4	80.61%	80.77%	0.14%	1.26%	0.522	51.49%
	16	0.125	0.5	5.7	78.52%	79.66%	0.14%	1.18%	0.514	51.88%
	32	0.125	0.5	8	75.01%	77.43%	0.11%	1.06%	0.507	50.41%
Step_size	8	1	0.71	2	81.66%	81.96%	0.17%	1.34%	0.524	51.67%
	16	1	0.5	2	81.89%	81.91%	0.14%	1.24%	0.525	51.89%
	32	1	0.35	2	81.64%	82.02%	0.15%	1.31%	0.527	51.78%
Step_size	8	0.5	0.5	2	83.09%	82.52%	0.14%	1.27%	0.527	51.60%
	16	0.5	0.35	2	83.09%	82.50%	0.14%	1.25%	0.528	52.25%
	32	0.5	0.25	2	82.98%	82.32%	0.14%	1.30%	0.530	52.03%
Step_size	8	0.25	0.35	2	83.70%	82.46%	0.15%	1.26%	0.528	52.17%
	16	0.25	0.25	2	83.53%	82.49%	0.18%	1.33%	0.529	52.71%
	32	0.25	0.18	2	83.44%	82.52%	0.17%	1.32%	0.524	51.67%
Step_size	8	0.125	0.25	2	82.98%	81.95%	0.16%	1.29%	0.525	52.34%
	16	0.125	0.18	2	82.91%	81.71%	0.17%	1.28%	0.527	51.55%
	32	0.125	0.13	2	82.88%	81.70%	0.17%	1.36%	0.526	52.34%
Time	8	1	0.5	1.4	83.27%	82.38%	0.15%	1.37%	0.528	52.04%
	8	0.5	0.5	2	83.09%	82.52%	0.14%	1.27%	0.527	51.60%
	8	0.25	0.5	2.8	82.40%	82.05%	0.16%	1.27%	0.525	51.88%
	8	0.125	0.5	4	80.61%	80.77%	0.14%	1.26%	0.523	51.49%
Time	16	1	0.5	2	81.89%	81.91%	0.14%	1.24%	0.525	51.89%
	16	0.5	0.5	2.8	81.61%	82.00%	0.15%	1.26%	0.527	51.99%
	16	0.25	0.5	4	80.89%	81.21%	0.13%	1.20%	0.521	51.59%
	16	0.125	0.5	5.7	78.52%	79.66%	0.14%	1.18%	0.514	51.88%
Time	32	1	0.5	2.8	46.65%	35.86%	0.14%	1.29%	0.523	52.10%
	32	0.5	0.5	4	79.26%	80.92%	0.14%	1.15%	0.519	51.37%
	32	0.25	0.5	5.7	77.90%	80.12%	0.12%	1.19%	0.514	50.84%
	32	0.125	0.5	8	74.60%	77.22%	0.12%	1.01%	0.510	50.14%
Time	8	1	0.71	2	81.66%	81.96%	0.17%	1.34%	0.524	51.67%
	8	0.5	0.5	2	83.09%	82.52%	0.14%	1.27%	0.527	51.60%
	8	0.25	0.35	2	83.70%	82.46%	0.15%	1.26%	0.528	52.17%
	8	0.125	0.25	2	82.98%	81.95%	0.16%	1.29%	0.525	52.34%
Time	16	1	0.5	2	81.89%	81.91%	0.14%	1.24%	0.525	51.89%
	16	0.5	0.35	2	83.09%	82.50%	0.14%	1.25%	0.528	52.23%
	16	0.25	0.25	2	83.53%	82.49%	0.18%	1.33%	0.529	52.71%
	16	0.125	0.18	2	82.91%	81.71%	0.17%	1.28%	0.527	51.6%
Time	32	1	0.35	2	81.64%	82.02%	0.15%	1.31%	0.527	51.78%
	32	0.5	0.25	2	82.98%	82.32%	0.14%	1.30%	0.530	52.03%
	32	0.25	0.18	2	83.44%	82.52%	0.17%	1.32%	0.524	51.67%
	32	0.125	0.13	2	82.88%	81.70%	0.17%	1.36%	0.526	52.34%
k	16	1	0.3	1.2	83.56%	82.62%	0.15%	1.29%	0.530	51.29%
	8	1	0.5	1.4	82.38%	82.38%	0.15%	1.37%	0.528	52.04%
	16	1	0.4	1.6	82.58%	82.22%	0.17%	1.40%	0.528	52.27%
	8	0.5	0.5	2	83.09%	82.52%	0.14%	1.27%	0.527	51.60%
	16	1	0.6	2.4	63.23%	57.12%	0.09%	1.09%	0.516	52.02%
	8	0.25	0.5	2.8	82.40%	82.05%	0.16%	1.27%	0.525	51.88%
	16	0.25	0.5	4	80.89%	81.21%	0.13%	1.20%	0.521	51.59%
	32	0.25	0.5	5.7	77.90%	80.12%	0.12%	1.19%	0.514	50.84%
	32	0.125	0.5	8	75.01%	77.43%	0.11%	1.06%	0.507	50.41%
Stochasticity	0.3	1	16	1.2	83.56%	82.62%	0.15%	1.29%	0.516	52.02%
	0.4	1	16	1.6	82.58%	82.22%	0.17%	1.40%	0.528	52.27%
	0.5	1	16	2	81.89%	81.91%	0.14%	1.24%	0.525	51.89%
	0.6	1	16	2.4	63.23%	57.12%	0.09%	1.09%	0.516	52.02%